DATA ACQUISITION SYSTEM FOR PHOTOACOUSTIC SYSTEMS

MS (Research) Thesis

By

K HARISHWAR REDDY

DEPARTMENT OF ELECTRICAL ENGINEERING
INDIAN INSTITUTE OF TECHNOLOGY INDORE

June 2021

DATA ACQUISITION SYSTEM FOR PHOTOACOUSTIC SYSTEMS

A THESIS

Submitted in fulfillment of
the requirements for the
award of the degree
of

Master of Science (Research)

by

K HARISHWAR REDDY

DEPARTMENT OF ELECTRICAL ENGINEERING

INDIAN INSTITUTE OF TECHNOLOGY INDORE

June 2021

INDIAN INSTITUTE OF TECHNOLOGY INDORE

CANDIDATE'S DECLARATION

I hereby certify that the work which is being presented in the thesis entitled **DATA ACQUISITION SYSTEM FOR PHOTOACOUSTIC SYSTEMS** in the fulfillment of the requirements for the award of the degree of **MASTER OF SCIENCE (RESEARCH)** and submitted in the **DEPARTMENT OF ELECTRICAL ENGINEERING, Indian Institute of Technology Indore**, is an authentic record of my work carried out during the period July 2019 to June 2021 under the supervision of Dr. Srivathsan Vasudevan, Associate Professor, Department of Electrical Engineering, IIT Indore.

The matter presented in this thesis has not been submitted by me for the award of any other degree of this or any other institute.

Harish. 23/08/21

Signature of the student with date
K HARISHWAR REDDY

This is to certify that the above statement made by the candidate is correct to the best of my/our knowledge.

V. Srivathsan 23/8/2021

Signature of the Supervisor of
MS (Research) thesis (with date)
Dr. SRIVATHSAN VASUDEVAN

K HARISHWAR REDDY has successfully given his/her MS (Research) Oral Examination held on ...23/08/21.....................

August 23, 2021
(Dr. Shanmugam Dhinakaran)
Signature of Chairperson (OEB) with date

V. Srivathsan 23/8/2021
Signature(s) of Thesis Supervisor(s) with date

23/08/2021
Signature of Convener, DPGC with date

Saptarshi Ghosh 23/08/2021
Signature of Head of Department with date
[HOD-EE (Officiating)]

Acknowledgment

I would like to express my sincere gratitude to my advisor Dr. Srivathsan Vasudevan for the continuous support of my MS Research study and related research, for his patience, motivation, and immense knowledge. His guidance helped me in all the walks of research and writing of this thesis.

I also extend my heartiest thanks to my thesis committee: Dr. Amod Umarikar and Dr. Gourinath Banda for their encouragement and insightful comments and also for putting up tough questions which helped me to widen my research perspectives.

This thesis could not be imagined without the help and support of Dr. M.S. Ansari from RRCAT Indore. I sincerely, take this opportunity to express my gratitude to Dr. M.S. Ansari and his team, especially Mr. Subhash and Mr. Abrat Verma for their out-of-the-way help, motivation, and guidance during my toughest phase of MS Research.

My heartfelt gratitude goes to my parents, who made all the sacrifices on my behalf, especially for their support and understanding. They have always been a source of inspiration and motivation for me throughout my life.

K Harishwar Reddy
MS (Research), II Year
Department of Electrical Engineering
IIT Indore

Abstract

Medical devices are rapidly becoming portable and mobile. The end-user anticipates that the devices would be simple to manage and run within arm's reach. On similar lines, we developed a portable data acquisition system-based sensing/monitoring device for the photoacoustic technique. In this technique, the Photoacoustic effect makes it possible to image opaque systems, especially biological samples and to analyze their conditions, deformities, and so on.

In the context of Photoacoustic Instrumentation, a single photodetector-based prototype photoacoustic scanner was incontestable to be a hit in early photoacoustic studies. Although imaging speed, system cost, and resolution are greatly enhanced, this type of traditional photoacoustic system is effective for collecting signals from a single sensor. But for imaging applications, it is essential to use multiple sensors at different locations in order to generate tomographical images. However, the biggest challenge is that for multiple sensors around the sample, we need multiple acquisition systems which makes the system bulky and also very expensive. Another challenge that comes with multiple acquisition systems is the difficulty to do online signal processing. Therefore, there is a strong need to build a low-cost data acquisition system that is compact especially to replace those oscilloscopes. Hence, a low-cost portable data acquisition system-based photoacoustic sensing/monitoring system has been proposed in the project to overcome the above-stated challenges.

The thesis discusses a detailed description of the proposed setup and its components. Lastly, applications of photoacoustic imaging are also discussed. The applications include both biomedical and non-biomedical applications.

TABLE OF CONTENTS

List of Figures

List of Tables

Chapter 1

Motivation and objectives

1.1 Introduction to Data Acquisition System

Data acquisition refers to the automated processing of data from sensors, instruments, and computers in a plant, laboratory, or area. Traditionally, data collection was done manually by writing down the readings of different instruments at specific times. Over the last few years, the use of Data acquisition systems (DAQ) in various aspects of data collection, control, and analysis has revolutionized modern-day science, production, and manufacturing. DAQ plays an important role to make a bridge between the physical world and the digital environment.

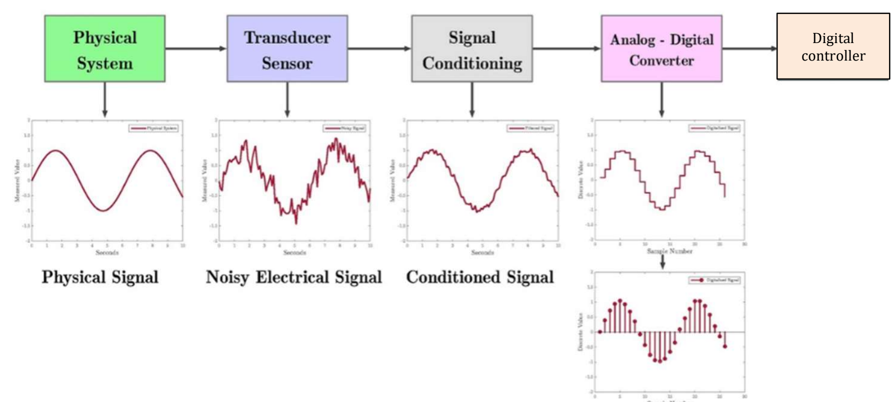

Fig. 1.1 Block diagram of a DAQ

Figure 1.1 depicts a DAQ block diagram. The physical phenomena or physical attributes to be measured is the first step in data collecting. Whatever physical property is being measured, the physical state must first be transformed into a unified form that can be sampled by a data acquisition system. Transducers are devices that are in charge of performing such transformations. A transducer is a device that is used to convert a non-electrical signal into an electrical signal. An acquisition system for measuring various qualities is dependent on the sensors that are capable of detecting those qualities. If the signal from the transducer is incompatible with the DAQ hardware, signal conditioning may be required. In most circumstances, the signal must be filtered, shaped, or amplified. Other signal conditioning examples include bridge completion, supplying current or voltage excitation to the sensor, isolation, and linearization. Signal conditioning ensures that the signal being monitored will not harm the device by protecting against overcurrent and overvoltage and tuning the input ranges to the analog to digital converter (ADC) input level. The ADC, which digitizes the conditioned signal with a specific resolution and sampling frequency, is the main component of DAQ hardware. DAQ has a processing unit or digital controller that sends the acquired data to the computer to be processed and analyzed.

Different DAQs require different customization as they are application-specific. The main criteria to take into account when selecting a data acquisition system are the maximum sampling frequency, the number of channels, input ranges, ADC resolution, and the possibility of simultaneous acquisition. DAQs with their subsystems like sensors, communication links, filters, preamplifiers, etc., have been demonstrated in various systems like an acoustic delay line module is proposed to improve the imaging quality and speed of low-cost photoacoustic tomography (PAT) system[1], Arduino-based low-cost data-logger system is designed for the monitoring PV system[2], implementation of low-cost acquisition technology in the field of vehicle engineering[3], virtual electronic system for measuring the EEG signals[4], etc. In addition to electric signals, these systems can measure temperature, acceleration, sound, force and pressure, light or location, and displacement. These data acquisition experiments and measurements may be mobile or fixed, used on a test cell or in extreme conditions in laboratory testing or for academic purposes.

DAQ plays a key role in portable applications, particularly in medical applications, because it allows for system mobility while reducing system complexity. These portable medical devices not only provide continuous and non-invasive monitoring of health parameters but also provide real-time updates to healthcare providers via connectivity. In this thesis, keeping in mind the role of DAQ in portable devices, a compact DAQ will be designed for photoacoustic imaging techniques.

1.2 Motivation and objective

Medical diagnostics has emerged as a completely new field in the world of medical sciences. It has become increasingly clear that detecting a disease or any pathological condition is critical in medical sciences. Identifying the right pathological state would result in appropriate treatment and therapy, and the patient would recover more quickly. For many severe conditions (e.g., cancer, immunosuppressive diseases, etc.), early diagnosis leads to fast and effective medication, which might mean the difference between life and death for the patient. Thus, the focus of diagnostic research during the last two decades has been on the development of biomedical imaging systems as well as early diagnosis. A typical biomedical imaging system includes a sophisticated chain of subsystems such as sensing, signal conditioning, acquisition, processing, and visualizing structural and functional images of living objects or systems.

The photoacoustic method (PAT), a biological imaging technology, has evolved significantly over the last decade, leading to several other exciting discoveries and applications. In addition, when compared to other techniques, this methodology has high sensitivity and accuracy in the diagnosis of a wide range of diseases. The basic physics of photoacoustic imaging is based on the conversion of light energy into sound. Briefly, Photoacoustic (PA) imaging is a non-invasive, hybrid imaging method that employs optical excitation and acoustic acquisition [5]. It is a pump-probe technique that irradiates the tissue sample using nanosecond laser pulses. When the temperature rises, the tissue releases the heat via acoustic (ultrasound) waves detected by an ultrasound sensor [6]. Multiple Ultrasound detectors and DSOs must be positioned around the tissue to acquire a photoacoustic signal in order to obtain the tomographic image from the acquired PA signal. The image is reconstructed using the PA data by inversely solving the photoacoustic equations. Furthermore, the ultrasonic sensor utilized for acquisition should be linked to an amplifier before being linked to an oscilloscope for signal acquisition. These modular instruments raise the overall cost of the system and make it cumbersome, making it unsuitable for clinical settings where a small training-free system is often sought. In addition, it is difficult to have a stand-alone system in a normal PA system for high-speed acquisition, monitoring, and normal recording characteristics like voltage and current through various sensors. Even though PA imaging offers numerous advantages for biological applications, this traditional PA system has yet to enter a clinical context.

The major objective of this thesis is to overcome these limitations and take this technique closer to the clinical benches by designing a compact and cost-effective Portable DAQ based Photoacoustic Sensing/Monitoring System to acquire the data with high accuracy and speed for reconstructing the tomographic image. The thesis also illustrates the technical approaches adopted to design the analog front end for signal conditioning the detected high-frequency PA signal whose amplitude is in a few microvolts.

1.3 Major contribution of the thesis

The thesis focuses on the development of a compact data acquisition system for a photoacoustic instrumentation system. As part of this, all of the DAQ's major components have been developed. The following are the thesis's key contributions to the development of those components:

- **The circuit design of high-frequency Analog to Digital converter for the proposed DAQ:**

  High ADC is an important component of the DAQ that is used to digitize the photoacoustic signal. This topic highlighted the need for high-frequency ADC for the proposed DAQ as well as the challenges involved with PA signal digitization. It also mentioned the requirement for additional components to provide a sharp transitional clock for the ADC. After choosing a suitable ADC, the hardware was built, and tests were performed on it to determine the effect of changes in input PA on ADC output. The linearity curve of the ADC output was also analyzed.

- **Digital Controller for the proposed DAQ:**

  There are several challenges associated with interfacing a high-frequency ADC with a microcontroller, such as generating a high-frequency ADC clock, synchronizing the DMA's GPIO sampling with the ADC conversion, and so on. This topic addressed the challenges encountered when acquiring the digitized PA with the STM32F446RE microcontroller. The hardware for the microcontroller was also built with the KiCad software tool.

- **Design of Analog front end for the Photoacoustic signal**

  The ultrasonic detectors detect the photoacoustic waves produced by the sample. The amplitude of a typical blood sample's PA signal is 0.6 mV. This shows that the signal power required for acquisition is relatively low, and that great resolution is required to capture even minor changes. Thus, in order to satisfy the input range of ADCs and analyze the wave, the detected PA signal must be prefiltered and amplified using the proposed system's analog front end. This topic went over the entire design specifics of a prefilter and a multistage amplifier to meet the above challenges and discussed the simulation results.

1.4 Overview of the thesis

This thesis consists of a total of seven chapters as mentioned below:

- Chapter 1 introduces the purpose and objectives of this thesis.
- Chapter 2 provides an overview of the Photoacoustic Imaging Technique and its instrumentation, as well as a discussion of the problems involved in the proposed PA system.
- Chapter 3 provides a detailed description of the circuit design of a high-frequency analog to digital converter for the proposed DAQ.
- Chapter 4 addresses the difficulties in collecting the digitized PA signal, as well as the choice of a digital controller to address certain difficulties in the proposed system.
- Chapter 5 discusses the design of a prefilter for the analog front end for PA signals, as well as the simulation results.
- Chapter 6 discusses the design and simulation results of a multistage amplifier for the analog front end of PA signals.
- Chapter 7 summarizes the thesis thereby giving some details about the prospects and their applications.

Chapter 2

Introduction to Photoacoustic Instrumentation

This chapter discusses the photoacoustic imaging technique and its associated instrumentation. It also discusses the limitations of conventional PA instrumentation and possible solutions through the proposed PA system.

2.1 Overview of Photoacoustic Imaging Technique

Biomedical imaging diagnostic techniques have evolved over a period of time to provide 1. Screening 2. Detailed diagnosis by providing vital information of the pathological condition 3. Continuous monitoring of the condition. The existing imaging techniques achieve high diagnostic precision and high quality in order to distinguish healthy and unhealthy tissue. Each type of imaging should have high contrast, good resolution, a high penetration profile, etc., as its fundamental parameters. The parameters listed above do not represent the current imaging methods. Table 2.1 presents the comparison of current imaging methods with the above parameters.

Technique	Contrast	Penetration depth	Resolution
Ultrasound	Acoustic impedance mismatch	~60mm	~300 micron
MRI	Magnetic field	~100mm	~100 micron
OCT	Optical scattering	~1-2mm	~10 micron
Confocal	Fluorescence / scattering	~0.2mm	~1-2 micron

Table 2.1: Conventional medical imaging techniques and their features

Table 2.1 shows that none of the techniques listed have the ability to meet the demand for advanced diagnostic techniques. As a result, research has inspired the development of a new imaging modality known as "Photoacoustic Imaging," which is a mixture of optical and non-optical techniques (optical and ultrasound) [8]. The sections that follow go into the photoacoustic technique and its associated instrumentation.

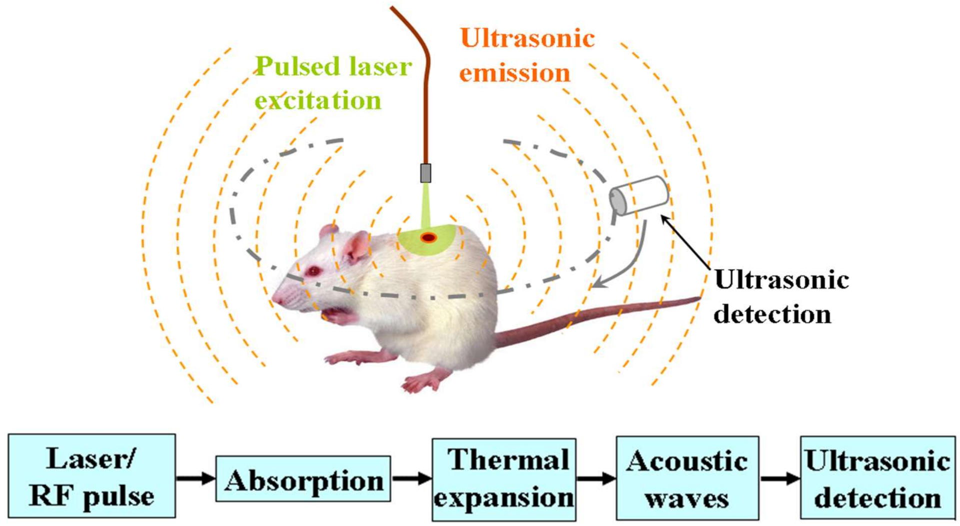

Fig. 2.1 Block diagram for PA signal generation and sensing by the ultrasonic detector

As the name implies, photoacoustic combines two distinct techniques: optics (photo) and acoustics (sound) [5]. PA imaging is a term used in medical science to describe the use of PA as an imaging diagnostic tool. It possesses all of the primary characteristics needed for any bio-imaging modality, including non-invasiveness, non-ionizing, high optical absorbance contrast, and sub-micrometer resolution in tissues and organs at greater penetration depths (> 5cm) [7,9]. It is based on the optical absorbance of hemoglobin, fats, melanin, water, and other tissue chromophores [5].

The PA effect is caused by the optical excitation of a sample, which generates an acoustic wave from the sample (further discussed in the subsection). The identification of acoustic waves makes this technique superior to traditional optical techniques because acoustic waves show less attenuation and scattering than light. As a result, PA imaging has less attenuation when compared to deep tissue imaging, making the technique capable of supplementing existing ultrasound imaging.

2.2 Photoacoustic effect

PA imaging is based on the PA effect. The excited sample absorbs the laser's energy, which is then converted into the kinetic energy of the sample molecules. This induces random motion and numerous collisions among the sample molecules, resulting in a large rise in temperature and sample expansion [7]. The sample relaxes again by dissipating the absorbed energy in a non-radiative way, which is known as a pressure wave or acoustic wave.

The ultrasound detector detects the acoustic wave and transforms it into an electrical signal, which is generally referred to as the PA signal. Since thermal energy is used to produce the stress wave in the sample, it is also referred to as a thermoelastic stress wave. The PA effect is depicted in Figure 2.1. The details of the optical source, absorption, PA generation, and detection are elaborated on in the following sections.

2.2.1 PA wave generation and propagation

Alexander Graham Bell first observed the fundamental physics behind the photoacoustic technique in 1880 during his work on photophone [11]. He discovered that sound waves are generated when the selenium cell is illuminated with modulated light. Since the incidence of light resulted in the production of sound, the physical phenomenon was named the photoacoustic effect.

The following are the basic requirements for producing PA waves:

- The laser energy irradiating the sample should be modulated.
- The laser source's wavelength must be within the spectrum of optical absorption of the sample's targeted chromophores.
- The sample should be exposed to laser energy for a short period of time (5-10 ns).

The PA effect can be seen in the sample if the above criteria are met. The modulated light beam penetrates the sample and is absorbed by the sample chromophores depending on its wavelength. Short-duration laser pulses are used to meet the sample's thermal relaxation time and stress relaxation time [10].

2.2.2 PA wave detection

The generated PA waves from the sample are typically propagated through a coupling medium and detected by an ultrasound sensor placed near the sample's surface. The ultrasound sensor converts the PA wave into an electrical signal, which is known as a PA signal.

The schematic of the PA wave generation and detection is shown in Figure 2.2. The sample absorbs heat from the laser source, as shown in Figure 2.2(a), and gradually expands, as shown in Figure 2.2(b) (b). Following that, it contracts back by releasing the gained energy in the form of acoustic waves (PA waves), which are detected by the ultrasound sensor to generate the PA signal depicted in Figure 2.2. (c).

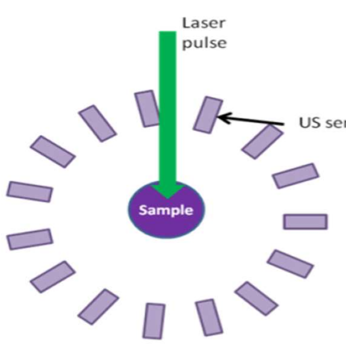

Fig. 2.2 (a)

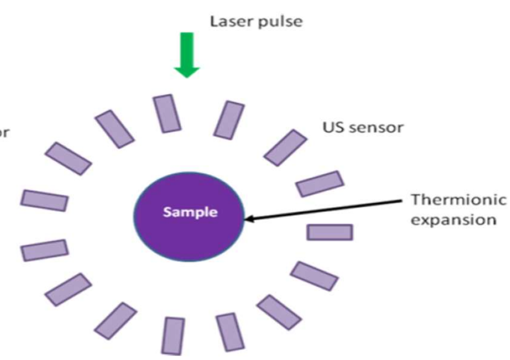

Fig. 2.2 (b)

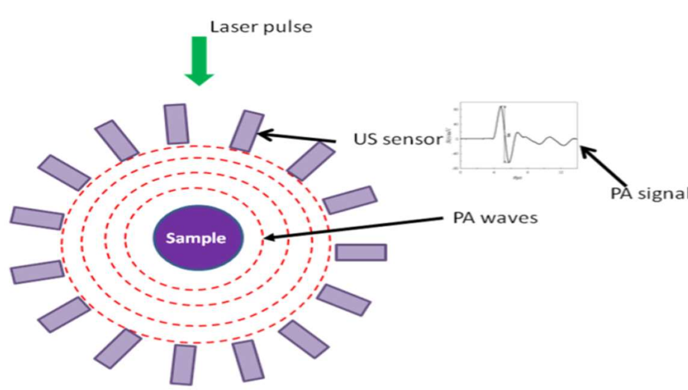

Fig. 2.2 (c)

Fig. 2.2 PA wave generation and detection (a). sample absorbing of heat from laser pulse, (b) sample expansion, (c) sample releasing PA waves

2.3 Ultrasound sensor

Ultrasound sensors based on piezoelectric crystals are primarily used in PA applications [5],[6]. These sensors work on the piezoelectric effect, which states that an applied potential difference between two ends of a piezoelectric crystal induces mechanical displacement and vice versa. Since acoustic waves are pressure waves, they exert a significant force, causing mechanical displacement in the piezoelectric crystal. The crystal converts this mechanical displacement into a voltage signal. The force (acoustic wave intensity) applied to the crystal determines the amplitude of the voltage signal [5].

The sensor's bandwidth and central frequency are determined by the thickness of the crystal used. To ensure electrical conductivity, the crystal is coated with a conducting material. Following that, electrodes are attached to the front and back sides of the crystal. Following that is the backing material, which dampens the sensor by absorbing the reflected acoustic signal. An acoustic insulator is used in the sensor to avoid the detection of external acoustic waves as well as internally produced acoustic waves in the crystal [6]. The entire setup is enclosed in an insulated shell. The crystal detects the PA signals and transforms them into electrical signals.

2.4 Characteristics of time-domain PA signal

PA waves are composed of compression and rarefaction since they are longitudinal waves. As a result, the piezoelectric ultrasonic sensor generates a bipolar signal that resembles the letter "N." Figure 2.3 depicts a standard PA signal from a circular simulated target.

Figure 2.3 clearly depicts the primary characteristics of the PA time-domain signal. It has four dominant features: amplitude (a), delay (T), width (τ), and relaxation period (χ). Width and relaxation time are two of these characteristics that are related to one another. These characteristics of the PA time-domain signal indicate very significant sample properties. For example, the amplitude of the PA signal is related to the sample's optical absorption and the amount of laser energy irradiated onto the sample, the delay provides information about the location of the absorber, the width of the signal reflects the size of the absorber, and the relaxation time depicts the sample's elastic property [31], [32]. As a result, the PA signal contains essential information about the sample. Only two functions, amplitude, and delay are used for image reconstruction. The signal amplitude appears as contrast in the picture, and the time delay provides information about the absorber's depth. Since normal and pathological tissues have distinct differences in optical absorption, PA imaging offers excellent contrast between these tissues [33], [35].

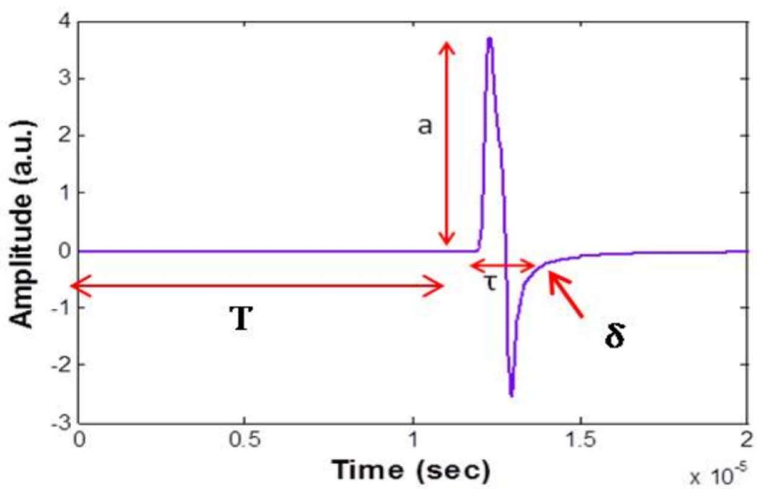

Fig. 2.3 A typical PA signal from a circular numerical target

2.5 Image reconstruction

2.5.1 Photoacoustic signal processing

The noise, as well as the sensor's bandwidth, have a significant impact on the PA time-domain signal acquired by the ultrasonic sensor, altering the actual profile of the PA signal. As a result, denoising and deconvolution with sensor response are needed to improve the signal-to-noise ratio (SNR) of the reconstructed image since PA image contrast is dependent on the amplitude of the PA signal [21], [22], [23].

All of these methods, such as averaging, filtering, and wavelet-based denoising, can be used to denoise PA signals. Random noise is typically removed by performing time averaging on the signal by performing multiple acquisitions from the same point. Averaging, on the other hand, is influenced by various artifacts such as patient movement, heart rate, and so on. To minimize the noise, other techniques such as moving time averaging and frequency filtering can be used [21]. When the signal is in the low-frequency regime, the moving averaging method is heavily used to eliminate high-frequency noise, while frequency filtering is applied to the signal with minimal overlap in noise and signal. Because the presence of multiple targets broadens the PA frequency spectrum, moving averaging is used to remove the high-frequency component, and frequency filtering is used to remove the useful frequency components that are overlapped with noise. As a result, wavelet-based denoising has gotten a lot of coverage. In comparison to Fourier transformation and other signal processing techniques, Wavelet decomposes a time-domain signal into a scalable window function with different coefficient values. By conducting transformation and scaling, a mother wavelet function is used to derive wavelet window functions. As a result, the wavelet transform is applied to the PA time-domain signal to minimize noise. The denoised signal is then recovered using the inverse wavelet transform.

Another important factor influencing the PA signal characteristics is the sensor's restricted bandwidth. Since the acquired PA time-domain signal is the convolution of induced acoustic pressure and the sensor's impulse response expressed as [21], this can distort the actual profile of the PA time-domain signal.

$$p_d(r,t) = p(r,t) * d_\delta(t) \tag{2.1}$$

Where d_δ is the sensor's impulse response

In the frequency domain, initial pressure is expressed as

$$p(r,\omega) = \frac{p_d(r,\omega)}{d_\delta(\omega)} \tag{2.2}$$

The inverse Fourier transform can be used to restore the original pressure profile. This, however, would greatly amplify the noise. As a result, the PA signal is deconvoluted using the zero routine and Wiener deconvolution. The equations below demonstrate both the zero routine and Wiener deconvolution [30]:

$$p(r,\omega) = \left[\frac{d_\delta^*(\omega)|p_d(r,\omega)|^2}{|d_\delta(\omega)|^2|p_d(r,\omega)|^2+\sigma_n^2}\right] p_{d(r,\omega)} \quad (2.3)$$

$$p(r,\omega) = \frac{d_\delta(\omega)p_d(r,\omega)}{d_\delta(\omega)^2+\delta^2} \quad (2.4)$$

2.5.2 Image reconstruction algorithm

Image reconstruction takes place after the acquired PA signal has been denoised. For image reconstruction, the processed PA signals are fed into various reconstruction algorithms such as back projection, time reversal, and the Fast Fourier Transform algorithm. The reconstruction algorithm determines both the image quality and the imaging speed.

Each element detects the amount of initial pressure in the case of back projection. Each acquisition point contains data on the point source as well as the total attenuation along the path. To reconstruct the image, the acquired data is projected back [24].

The advancement of the reconstruction algorithm results in more accurate reconstruction and improved computational performance. Back projection, for example, is updated to filtered back projection, which employs filtering before or after the back projection stage. The artifacts in the reconstructed image are reduced as a result. Although this algorithm is computationally effective, it is limited in practical application to spherical geometry [25].

The time-reversal algorithm, on the other hand, reconstructs images by using the temporally reversed PA waveform obtained from each detection point [20]. To trace the origin of a specific point source, PA signals acquired by each sensing point are temporally reversed and numerically retransmitted in the medium. The primary benefit of this algorithm is that it needs the fewest assumptions and applies to any geometry [26], [27]. However, the time-reversal algorithm requires a large amount of memory for computation, which restricts its practical use. An effective technique known as the pseudo-spectral K-wave propagation model [28], [29] reduces the memory requirement of the traditional time reversal technique. This makes use of a forward model pre-computation of initial pressure. The use of matrix-based and simulated p_0 would then minimize the amount of memory required for computation.

2.6 Types of PA techniques

The PA technique is primarily used in the biomedical field for imaging applications. However, this has also been investigated for spectroscopy (gas and liquid analysis) and a few applications on PA signal analysis. PA technique can be divided into three broad applications: imaging, spectroscopy, and PA signal analysis. PA imaging is further subdivided into two types: PA tomography and PA microscopy [12],[13]. PA imaging is done with an ns-pulsed laser as the excitation source; however, some reports have documented the use of laser diodes in PA imaging.

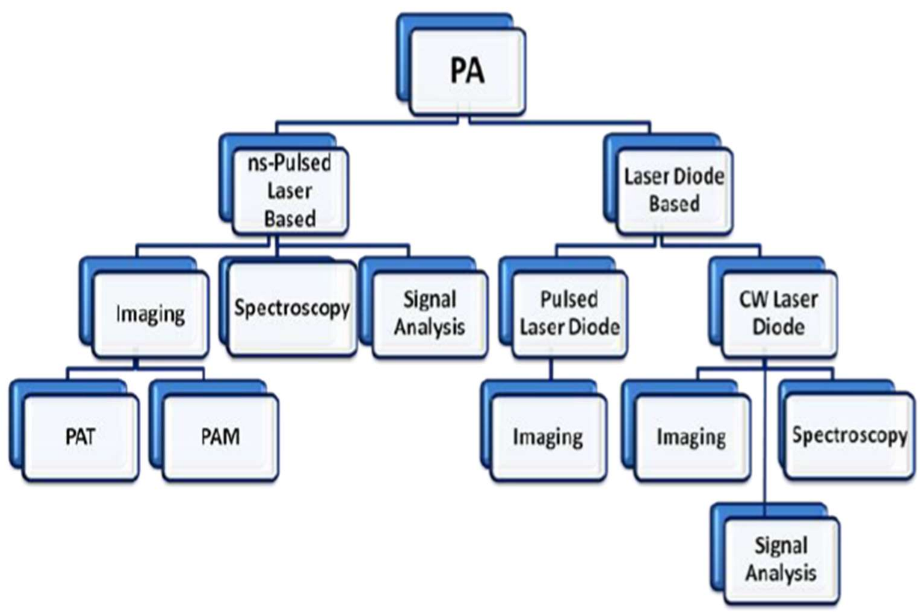

Fig. 2.4 Typical modalities of PA techniques explored

2.6.1 Laser diode-based Photoacoustic Imaging

For non-ionizing functional and molecular imaging of humans and small animals, photoacoustic computed tomography (PACT) has been extensively studied. A bulky and expensive tunable laser is usually used to penetrate deep inside tissue. For photoacoustic imaging, laser diodes have recently emerged as a cost-effective and compact alternative illumination source. Most PACT systems currently use Q-switched, nanosecond pulsed tunable lasers based on Nd: YAG (neodymium-doped yttrium aluminium garnet)/OPO (optical parametric oscillator) and a multichannel ultrasound detector array with associated data acquisition hardware. These lasers normally produce hundreds of millijoules of pulse energy to achieve an adequate photoacoustic signal-to-noise ratio from targets several centimeters deep within the tissue, such as the deep vasculature of the human breast. The clinical application of these lasers is limited due to their high cost and bulk. When the intended application needs a 2 cm imaging depth, high pulse energy lasers with a low pulse repetition frequency (20 Hz) can be replaced for low pulse energy lasers with high pulse repetition frequencies (>1 kHz). Many researchers have used laser diodes to create low-cost photoacoustic imaging systems in order to achieve this aim.

2.6.2 Nano-second pulsed laser-based Photoacoustic Imaging

The sample is irradiated with a nanosecond (ns) pulsed laser, which produces broadband PA waves that are detected by the ultrasound sensor and converted into the desired PA signal. This PA signal can be combined with various signal processing and image reconstruction techniques to generate the desired sample image [12],[13]. PA imaging is further classified into PA tomography and PA microscopy.

2.6.2.1 PA Tomography

PAT, also known as optoacoustic or thermoacoustic tomography, is the fundamental PA imaging technique in which an ns-laser pulse produces spherical acoustic waves from the sample. To collect the acoustic waves, either a single element ultrasound sensor is scanned through the entire sample, or an array of ultrasound sensors in a particular geometry is used. While the first method of scanning is time-consuming and requires repeated heating of the sample, the second method is expensive and complex. Besides this, the geometry of the sensor array is chosen based on the form of the sample [14]. Moreover, these PA signals are combined with image reconstruction algorithms to generate the PA image.

2.6.2.2 PA Microscopy

PAM is the only PA technique that can visualize blood vessels at a sub-micrometer scale. Unlike PAT, PAM generates the image using a centered single-element ultrasonic sensor that is scanned across the sample. As a result, PAM does not necessitate the use of any robust image reconstruction algorithm. Alternatively, the ultrasonic sensor is fixed and the directed laser beam is scanned alongside the sample. PAM is known as optically resolved PAM (OR-PAM) or acoustically resolved PAM (ARPAM) based on the scanning mechanism [15]. The lateral resolution of the PAM is determined by the relative size of ultrasonic or optical focus, while the axial resolution is determined by the time-resolved PA signal [16]. PAM can be used for image-guided surgery and treatment as well as detailed imaging. However, since the image resolution and penetration depth in PAM are scalable, the penetration depth is restricted in order to achieve sub-micrometer resolution.

Several studies on the samples are carried out using a Nano-second pulsed laser in this thesis.

2.7 Photoacoustic Instrumentation

2.7.1 Instrumentations for PAI

Based on an ultrasound (US) imaging system, VisualSonics developed the Vevo LAZR photoacoustic platform for small-animal preclinical imaging. The major benefits of in vivo real-time imaging are ease of control and whole-body imaging. Nexus 128 was also made by Endra Life Sciences for preclinical cancer PAI in small animals. A built-in analysis software package in this framework, which produces high-resolution PAI pictures, can be used to acquire advanced two-dimensional (2D) and three-dimensional (3D) images. With

Endra Nexus, Van de Sompel et al were able to increase image quality in both phantom and tissues by correcting temperature changes.

In addition, PAI instruments MSOT (multi-spectral optoacoustic tomography) and LOUIS-3D were developed by iThera Medical and Seno Medical Instruments, respectively. The MSOT Acuity was developed by iThera Medical with a fast-tunable 50 Hz laser and 2D and 3D detectors and has been shown to achieve real-time biomedical imaging and quantitative imaging of lesions through tissue chromophore distribution and concentration. When comparing the two detectors, the 2D probe outperforms the 3D probe in terms of signal loss and anatomical similarity, while the 3D probe excels in rapid 3D imaging, allowing visualization of superficial areas. Furthermore, the Twente Group created a dual-imaging modality in collaboration with ESAOTE Europe BV by combining a US transducer array and a diode stack laser in a single US probe connected to a commercially available US device. The new imaging modality combines the benefits of both US and PAI, with the US providing anatomic data and PAI providing functional information. It should be noted that PA scanners have been applied in clinics as a prototype for augmenting the US techniques such as sentinel lymph node (SLN) dye injection.

Instrument	Modality	Advantage	Application
LAZR(VisualSonics)	Ultrasound photoacoustic imaging integrate	Whole-body with sectional PAI options	Preclinical
Nexus 128 (Endra Life Sciences)	Photoacoustic imaging	Fast imaging and high-resolution 3D image reconstruction	Preclinical cancer detection
MSOT (iThera Medical)	Photoacoustic tomography	Real-time, whole-body tomography with body navigations	Preclinical whole-body PAI especially cancer detection and brain imaging
LOUIS-3D (Tomo wave Laboratories Inc.)	Photoacoustic imaging with tunable laser switch	The first PAI scanner for SLN dye injection guidance	Preclinical and clinical studies on oncology, vascular angiography, hematology, etc.

Table 2.2: Typical commercial PAI instrumentations for preclinical and clinical [36] studies

2.7.2 Conventional Photoacoustic system

The general experimental setup for the PA imaging for a single sensor is shown in figure 2.5. Nano-second Nd: YAG pulsed laser is used as an excitation source to irradiate the sample. Upon irradiation, there is a temperature excursion that creates a PA signal. The generated PA signals propagate through a water medium and are captured by an ultrasound detector. The detector is guided around the sample by a stepper motor to collect the PA signals at various points. For effective ultrasound coupling, both the sample and the ultrasound detectors are immersed in water. The acquired photoacoustic signals are then digitized by a DSO and transferred to a computer for tomographic image reconstruction. The final tomographic image quality is independently influenced by eight system parameters associated with the ultrasound detector, namely, element number, view angle, aperture size, focusing, bandwidth, center frequency, scan step angle error, and orientation error [21]. The image reconstruction approach used in this study is based on single-variable analysis, which allows only one parameter to differ while keeping all others constant unless otherwise specified.

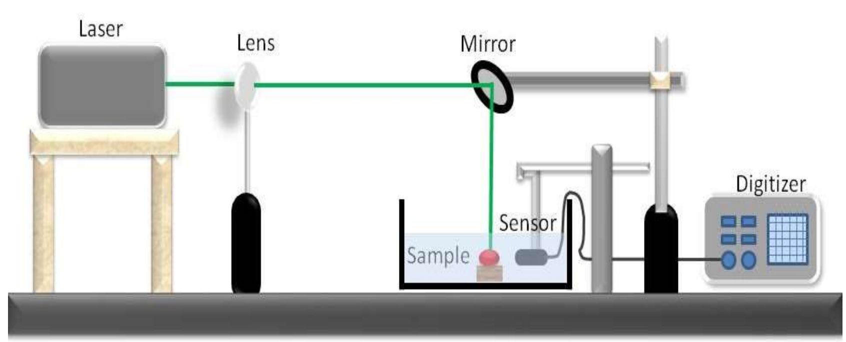

Fig. 2.5 Experimental Setup for the acquisition of PA signal from a single sensor

This single-detector-based prototype PA scanner was incontestable to be a hit in early photoacoustic studies. Even today, it is still frequently employed in many photoacoustic experiments for proof-of-concept studies because of its simplicity, and effectiveness. Although imaging speed, system cost, and resolution are greatly enhanced, trendy PA scanners work equally to this proposed prototype. This type of traditional PA system is effective for collecting PA signals with a single sensor.

For imaging applications, it is essential to use multiple sensors at different locations in order to generate tomographical images. However, the biggest challenge is that for multiple sensors (Fig. 2.6) around the sample, we need multiple acquisition systems (e.g., oscilloscope) which makes the system bulky and also very expensive. This is particularly important from an Indian context. Therefore, there is a strong need to build a low-cost data acquisition system that is compact. The challenge is that the bandwidth of the sensor is around 20 MHz and hence as per Nyquist criteria the data acquisition system should support the data transfer whose frequency is more than 40MHz. Another challenge is that doing online signal processing with multiple sensors is difficult. Hence, a low-cost portable DAQ based PA sensing/monitoring system has been proposed in this thesis to overcome the above-stated challenges.

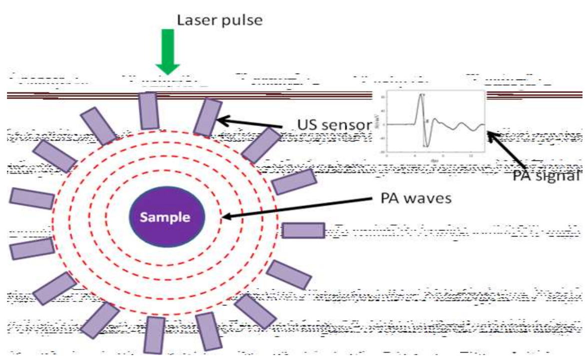

Fig. 2.6 Installation of multiple sensors around the sample

2.7.3 Proposed Photoacoustic system

The two key features of the proposed DAQ system are to acquire a high-speed signal with an amplitude of a few microvolts and to replace DSO with DAQ. Figure 2.7. depicts the functional block diagram of the proposed PA system. It primarily consists of an analog front end followed by a DAQ unit. The various stages of the proposed system are briefly discussed below.

The key motivation for this work is the need for a fast and reliable analog front-end design (AFE) to amplify and digitize the PA signal for further processing. The AFE conditions the sensor's output, whose amplitude is in few microvolts, and uses the AD9283 ADC to perform analog-to-digital (A/D) conversion at

50MHz. In this application, the STM32F446RE microcontroller is used to obtain high-speed and accurate data from the ADC. The signal is averaged over 50 frames using the microcontroller to minimize random noise in the signal. This time-averaged data is then transferred to a computer through a serial port for image reconstruction, real-time monitoring, and display.

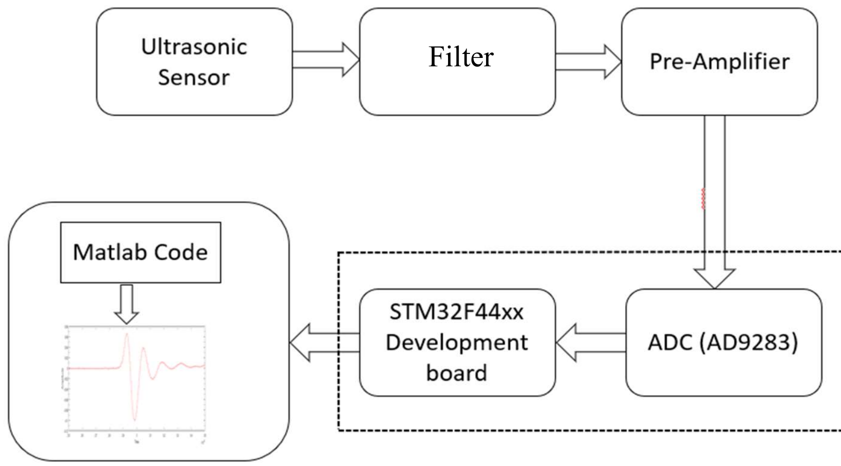

Fig. 2.7 Block diagram of a proposed low-cost DAQ system

2.7.4 Challenges and objectives

The following are the few challenges in the proposed system.

- It is difficult to obtain PA signals since their amplitudes are in the microvolt range.
- PA signals are available at high frequencies ranging from 1Mhz to 5Mhz, where noise dominance is high.
- Achieving high gain in the wide frequency range is very difficult using the single-stage amplifier due to the gain-bandwidth limitation.
- Difficult to digitize and acquire the data on the microcontroller since parasitic capacitances play a vital role in degrading the signal strength.

The two key designs that must be understood to address the above challenges for the implementation of the proposed PA system are as follows.

- Design of Analog front-end (AFE)
- Acquisition of PA Signal on the digital controller

Both the topics will be covered extensively in the following chapters.

Chapter 3

Design & Development of Data Acquisition System: Analog to Digital Converter

3.1 Motivation

This chapter focuses on the challenges faced in the development of a data acquisition system for a photoacoustic instrumentation system. Fig. 3.1 shows a typical PA signal obtained from a blood sample.

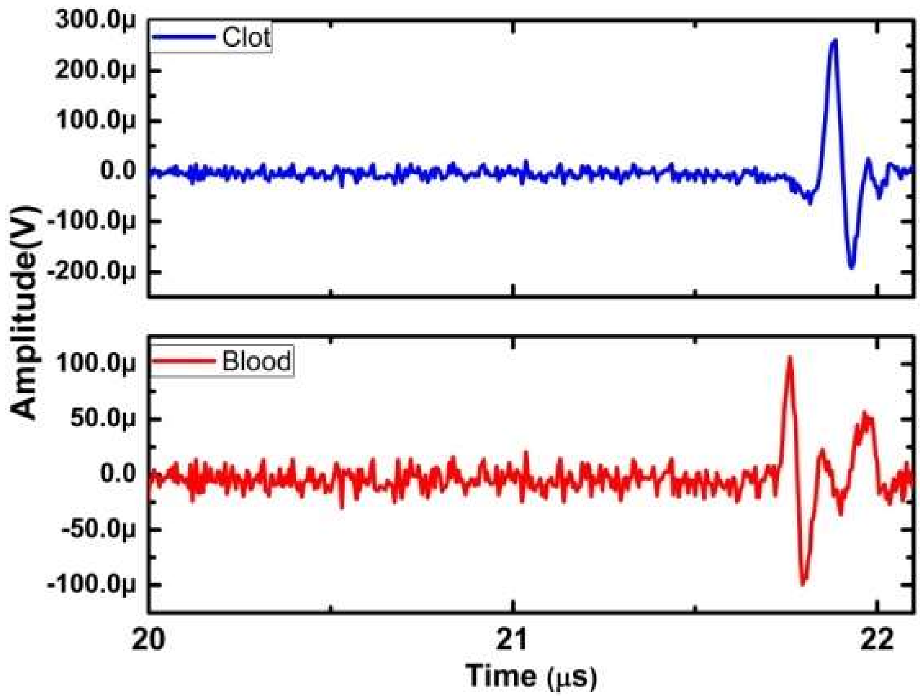

Fig. 3.1 PA signals obtained from the blood sample and a blood clot of a patient

The important features of PA signal that would be taken into consideration for diagnosing if the sample is normal or not are

- The peak amplitude of the PA signal
- Rise and fall time of the PA signal
- Time taken for the PA signal to appear would be used for tomographical applications

It is worthwhile to note from Fig. 3.1 that the amplitude of the PA signal of a typical blood sample was 0.3 mV on the positive side and similar on the negative side. This shows that the signal power that needs to be acquired is very low and that requires very high resolution to capture even small changes. On the other hand, the PA signal of a typical blood clot consists of 0.1 mV as peak amplitude on both the positive and negative sides. Even though amplification can be applied to these signals, the noise levels would also increase post-amplification. Hence, the power of the signal poses a serious concern on what kind of analog to digital conversion would be used. Moreover, in order to capture accurately the rise and fall time of the signal, several data points are needed within 0.2 to 0.3 microseconds. Based on these results, the following are major requirements:

- Resolution of the Analog to digital converter (ADC) would be determined by the amplitude of the PA signal
- Rise and fall time data points would determine the acquisition speed of the ADC

3.2 Conventional acquisition strategy

The majority of DAQs use on-chip ADC microcontrollers. However, in on-chip ADCs, there is a tradeoff between speed and resolution. Additionally, the following are some of the drawbacks of an on-chip microcontroller ADC peripheral.

- On-chip ADC microcontrollers have a limited conversion rate of about 10 MSPS.
- The internal reference voltage for an ADC in the microcontroller is either derived from the main microcontroller power supply (usually VCC) or a dedicated analog reference voltage pin. But the ADC output's accuracy is dependent on an accurate and stable reference voltage. To avoid noise interference, the internal reference voltage must be kept separate and isolated from the high-speed digital logic.
- A higher reference voltage may be used to reduce the influence of noise, but the resolution must be improved to preserve the same precision when calculating low voltages. This would increase the area of the ADC on

the microcontroller die as well as the ADC testing time during development, all of which would raise the cost of the microcontroller [37].

- Any peripheral on a microcontroller must deal with the benefits and drawbacks of the process technology upon which the semiconductor is designed. Timers, parallel I/O ports, and communication interfaces like SPI, I2C, and UART interfaces are all very compatible with CMOS digital process technology [37]. An ADC, on the other hand, is an analog peripheral. Internally, analog peripherals such as ADCs and comparators necessitate the use of a capacitor [37], which is not possible on a pure digital method. This necessitates the use of mixed-signal process technology. Since a microcontroller is primarily a digital semiconductor with high-speed requirements, the mixed-signal technology used must not sacrifice digital speed for analog functionality or performance characteristics. Although this juggling act is possible for popular applications, it can restrict the efficiency of analog peripherals in high-end analog applications. Devices with more analog logic, such as single-chip ADCs, can only have slow digital logic.
- Another difficulty for microcontroller ADCs is to be used in applications that require high precision over a wide range of resolutions. Applications that use 24-bit ADCs and need accuracy greater than 2 LSBs, for example, require very accurate and stable reference voltages and experience some of the same issues as those mentioned above.

Hence, small external ADCs are used in portable spaces where high frequency, high performance and sensitivity, and enhanced noise immunity are needed to overcome the above problems. These external ADCs with specific features or performance characteristics are being produced by companies such as Texas Instruments, Analog Devices, and others.

In this application, an external ADC operating at a conversion rate of 50 MSPS is used to obtain very accurate data from the sensor. The choice of an external ADC for this DAQ as well as its features are discussed in the following section

3.3 Choice of an ADC

In our experimental lab, PA signals were acquired using various ultrasound detectors. Their bandwidth varies from 7MHz to 20MHz. The ADC's conversion rate should follow Nyquist's criterion. There are several types of ADCs available to meet the above criteria, each with its own set of advantages and disadvantages. Understanding the needs is the most important factor in selecting the best ADC.

The following important attributes are essential when selecting the best ADC for this DAQ.

- Should be able to sample the input PA signal should happen at every clock edge.
- Should have the conversion rate greater than 50MHz
- Should have an adjustable input range.
- Required ADC resolution of greater than or equal to 8 bits
- A minimum amount of control, power, and data signals
- It should provide an easy-to-use parallel communication interface for data access. Since the advantage of a parallel A/D converter is its relatively quick real-time conversion rate. Apart from the quick conversion rate, the time-averaging approach can also be applied to the digital data to improve the signal-to-noise ratio (S/N ratio) by reducing the random noise associated with the PA signal. This method can be extended to any case where the signal stays constant over many measurement cycles. Here the PA signal is recorded several times and averaged in the microcontroller. Consequently, the noise will eventually cancel out because it contributes in a probabilistic fashion, while the net signal still contributes to a signal in the same direction.

AD9283 is one of the ADCs that meets the above specifications. So, it has been selected for this application. It is a low-cost, low-power, small-size, and easy-to-use 8-bit monolithic sampling analog-to-digital converter with an on-chip track-and-hold circuit. The product converts at a rate of 50 MSPS and has excellent dynamic efficiency across its entire operating range. Besides that, as shown in Figure 3.2, it can sample the input PA signal should happen at every clock edge and streams out 8 bits of latched data outputs with four pipeline delays in each conversion process.

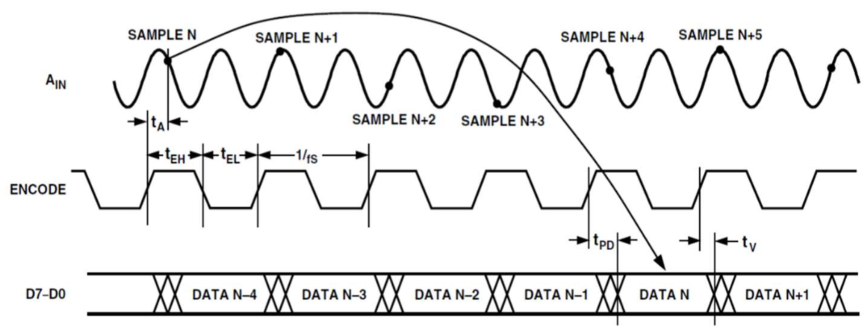

Fig. 3.2 Timing Diagram of the AD9283 ADC [38]

3.4 Theory of Operation

Figure 3.7 shows the schematic diagram of the ADC circuit. The Amplified PA analog signal will be applied at pin number 6 of AD9283 [38] as a single-ended input. It also allows the most flexible use of ac or dc and differential or single-ended input modes. For peak performance, the inputs are biased at 0.3 × VD. The nominal input range is 1.024 V p-p.

Fig. 3.3 Generation of a sharped transitioned clock for the ADC at high frequency

As previously stated, the bandwidth of ultrasound detectors ranges from 7MHz to 20MHz. Therefore, to meet the Nyquist requirement, a conversion rate of at least 40MHz is needed. Figure 3.3 shows the ADC receiving the same rate clock from the microcontroller to achieve the specified conversion rate. However, at high frequency, the generated clock exhibits slew.

Fig. 3.4 Input and output of the SN74LVC IC on Oscilloscope

Any timing jitter in the clock would be combined with the desired signal and degrade the ADC's high-frequency performance. In this application, an XOR gate (SN74LVC IC) is used to remove the slew present in the produced clock from the external source. It is a quadruple 2-input exclusive-OR gate with a VCC range of 2.7 to 3.6 V [39]. It takes the clock from an external source as one of its inputs and produces the sharped transitioned clock for the ADC at its output. Here XOR gate takes the clock as input from the STM32 microcontroller, which has a frequency of 5 MHz and generates a sharped transitioned clock for the ADC. Figure 3.4 shows the input (blue) and output (yellow) waveforms of an XOR gate on DSO. A similar level of performance is observed from the XOR gate at about 50MHz.

Figure 3.7 shows the schematic of the AD9283 ADC circuit. When it receives the clock, the ADC produces digital outputs that are TTL/CMOS compatible. But at such a high-frequency SNR of digital outputs is very less and it is difficult for the digital controller to acquire the ADC output. To ensure that ACQ/ACTQ574 is used which guarantees simultaneous switching noise level and dynamic threshold performance. The ACQ/ACTQ574 consists of eight edge-triggered flip-flops with individual D-type inputs and 3-STATE true outputs. The buffered clock and buffered Output Enable are common to all flip-flops. The eight flip-flops will store the state of their individual D-type inputs that meet the setup and hold time requirements on the LOW-to-HIGH Clock

(CP) transition. With the Output Enable (OE) LOW, the contents of the eight flip-flops are available at the outputs. When OE is set to HIGH, the outputs go to the high impedance state. Operation of the OE input does not affect the state of the flip-flops.

The ADC needs only a 3.0 V (2.7 V to 3.6 V) power supply and an encode clock to operate at full performance. The output buffers are powered from a separate supply, allowing adjustment of the output voltage swing to ease interfacing with 2.5 V or 3.3 V logic. Care should be taken when loading the digital outputs of any high-speed ADC. Large output loads create current transients on the chip that can degrade the converter's performance. The PCB design for this circuit is done on the KiCad software tool and is discussed in the following section.

3.5 Introduction to KiCad

KiCad is used for designing circuits and printed circuit boards. Its software combines schematic capture, custom symbols and libraries, PCB design, calculators, and useful tools into a single package. It is an open-source platform that is continually developing and includes complex features such as microwave traces and multilayer PCBs.

When a new project is created on KiCad, two new files are created: a schematic file and a PCB file. Creating schematic files often results in the PCB file being generated automatically. Its schematic files have the extension ".sch," and KiCad PCB files have the extension ".kicad_pcb," [40].

The steps to take after creating a new project in KiCad for PCB design are listed below.

- eeschema – The schematic editing program
- Schematic library editor – For making new libraries
- Pcbnew – The PCB editing program
- PCB Footprint editor – For creating new PCB footprints
- GerbView – Gerber viewer
- Bitmap2Component – Convert an image into a PCB component (logos e.g.)
- PcbCalculator - Calculator program for various applications

- PI Editor – For creating custom sheets

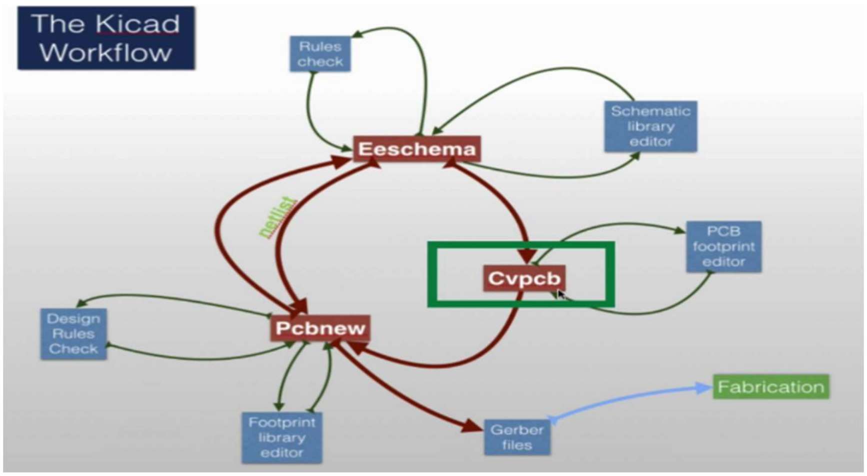

Fig. 3.5 KiCad's design flow [40]

3.5.1 Schematic design

When working with KiCad, a design flow is adopted that is similar to that of most other programs.

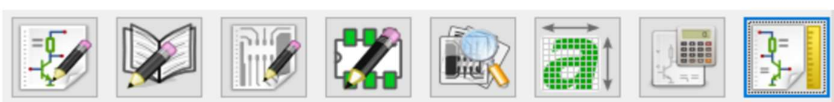

Fig. 3.6 *KiCad's application toolbar[40]*

The eeschema software is used to create the schematic in the first level. Eeschema is used to produce an electrical schematic that defines the circuit that will ultimately be printed on the PCB board. The schematic is generated by selecting components from the library and creating components that do not exist in the library using the schematic library editor. Later part numbers are allocated to components after they have been placed and wired together, which can be achieved manually or automatically using optional numbering schemes.

The electrical rules search is run at some point during the design of this schematic to identify any obvious mistakes or electrical mistakes in the design. The electrical rules search will generate a defect report, which will be used to fix any problems in Eeschema. Once all is correctly laid out and there are no more errors in the schematic, proceed to the Pcbnew application to begin doing PCB layout design.

After the parts have been numbered, a component file is created that contains a list of all the parts as well as a netlist of how they connect together. Figure 3.7 shows the schematic of the AD9283 ADC circuit. Then, from eeschema, a special software called CvPCB is launched, which is used to pick PCB footprints for each part. After selecting the footprints, the netlist is exported and Pcbnew is loaded. After selecting the footprints, the Pcbnew is loaded and the netlist is imported.

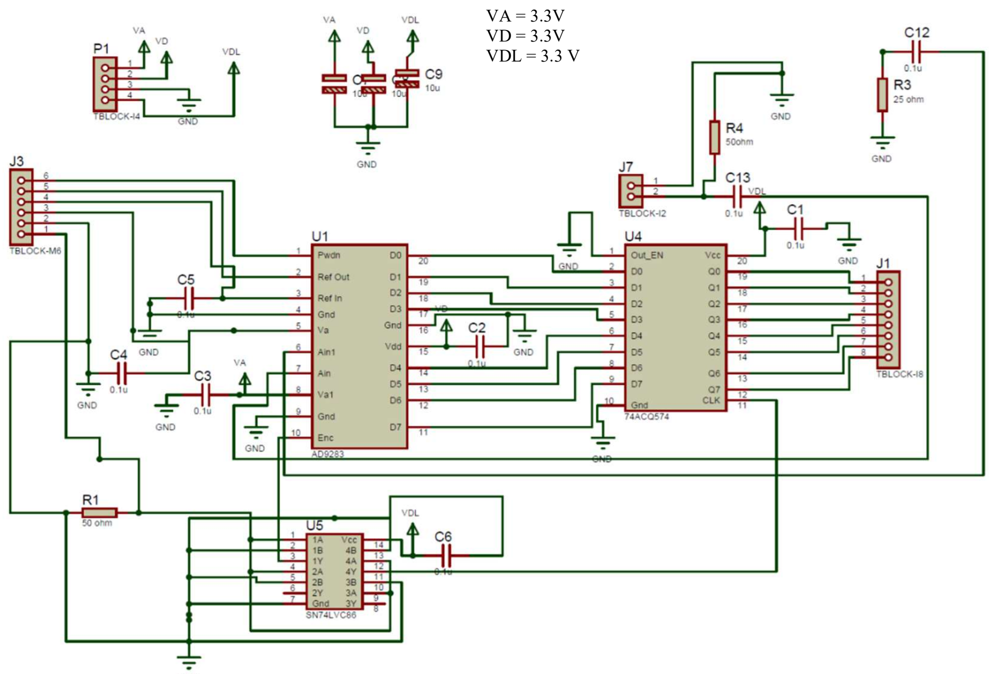

Fig. 3.7 Schematic diagram of the ADC circuit

3.5.2 PCB Layout Design

To create the final PCB, the components are positioned, oriented, and routed. Although KiCad does not provide an auto-router, there is a free auto-router available that performs surprisingly well. The PCB design for ADC is done on KiCad following the design flow steps.

The following are the few rules followed in this PCB layout design.

- Decoupling capacitors are placed near the power pins of ADC IC. These are used to prevent disturbances from various sources. Synchronized logic and data buses can produce large instantaneous current flows with large loads from the local power supply systems (PDS). In the event of such instantaneous loading, the inductance in the PDS prevents the design power supply from supplying additional current instantaneously, causing local supply voltage to fall or ring. So, the placement of decoupling capacitors is crucial to mitigating voltage fluctuations.

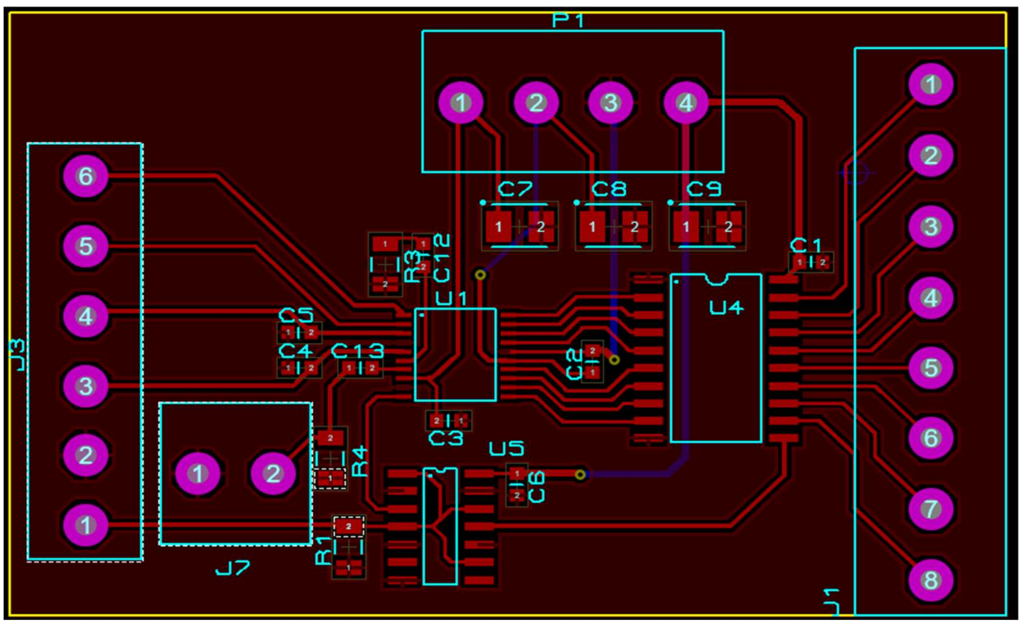

Fig. 3.810 PCB layout design

- Since the ADC operates at a low current, the track width in the layout is kept to a minimum. Furthermore, the low track width will reduce parasitic losses. The minimum trace size should be kept at 7mil. 10mil is the recommended size for the traces but 7mil or 8mil can be accepted. Power lines are kept comparatively thicker. For max 100mA, use 12mil; for max 500mA you can use 16mil, and so on.

- Tantalum capacitors (TC) are used to minimize variance in capacitance characteristics at power supply pins. Unlike ceramic capacitors, these undergo very little change in capacitance characteristics due to circuit DC voltage and/or temperature variations, reducing the need to check the effective capacitance.

- A two-layered PCB with separate layers of power and ground is designed. The VDD, VSS pins of the various ICs can be directly connected to the power planes thus reducing the tracks needed to connect the supply and ground. Longer tracks will have a high inductive effect.
- The shorter the lead between high-frequency circuit pins, the better. The intensity of the signal's radiation is proportional to the length of the signal line's routing. The longer the high-frequency signal lead, the easier it is to connect to its components. As a result, the shorter the routing length needed for high-frequency signal lines such as signal clock, crystal oscillator, DDR data, LVDS, USB, and HDMI, the better.
- The less bend between high-frequency electronic device pins, the better. High-frequency electrical wiring leads should be fully straight. A 45-degree broken line or arc break may be used if a break over is needed. This requirement is only used to increase the bonding strength of copper foil in low-frequency circuits while meeting this requirement will minimize external emission and coupling of high-frequency signals in high-frequency circuits.
- When wiring, any kind of high-frequency signal does not form a loop. If it is unavoidable, keep the loop area as small as possible.
- If there is significant crosstalk between two lines, a ground line or ground plane may be added to play the function of separation and minimize crosstalk if the cabling space allows

If the PCB has been laid out and all connections have been made, run a design rules review to ensure that, for example, run a design rules analysis after the PCB has been laid out and all links have been made to ensure that, for example, a track is not too close to a pad and other such things. Look for any broken or disconnected pads, as well as something else of the sort. One thing to keep in mind is that always use the footprint editor to patch footprints. To make it, the PCB data must be exported as a list of files known as "Gerber files." Gerber files contain several similar files, one Gerber file for each layer of the PCB, and contain instructions that the fabrication house would need to produce the PCB.

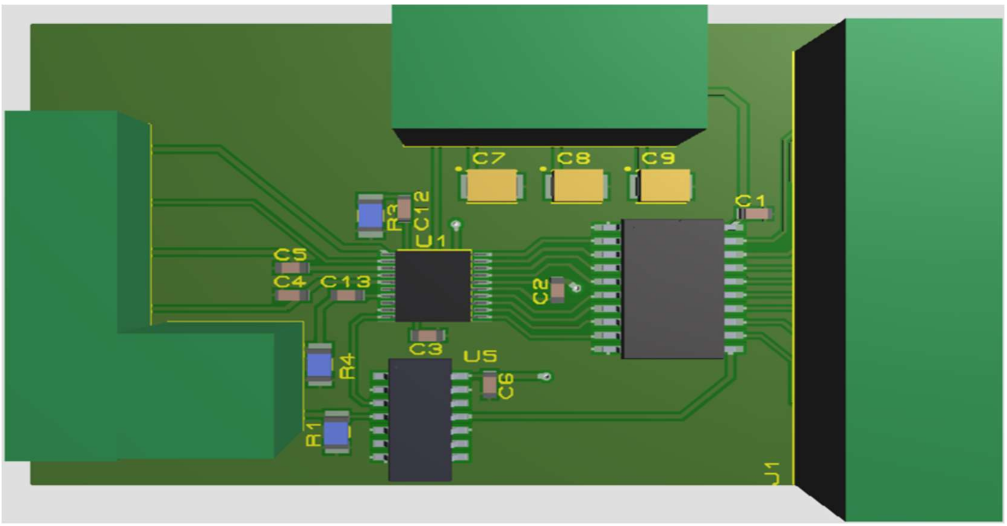

Fig. 3.9 3D Model of PCB design

3.6 Experimental setup and its results

Two main experiments are carried out in order to validate the ADC circuit. One is testing the stand-alone ADC IC, while the other is using the ADC IC in conjunction with all other supporting components.

In the first experiment, the ADC is standalone which can be seen in figure 3.10.1. As previously mentioned, when a system is operating at high frequency, a minor error in the circuit design can affect device performance due to noise. The same thing happened here, as seen with the result shown in figure 3.10.2. The flaws in this circuit's design are the placement of decoupling capacitors that are too far away from the power pins and the digital outputs have uneven track maintenance. In addition, the input clock has a high slew since there is no XOR gate to produce a sharp transitioned clock to ADC. All of these errors have affected ADC's performance.

To validate the ADC circuit, the zero-volt signal is applied as an input to it from the DC power supply. The ADC clock is given from the microcontroller whose frequency is 5MHz. The MSB of the ADC should be logic high and all others should be logic low at the output for the given input. However, most of the output bits are toggling randomly due to flaws in the circuit design which is not desirable. The outputs D7 and D6 of the ADC are collected on oscilloscope and can be seen in figure 3.10.2.

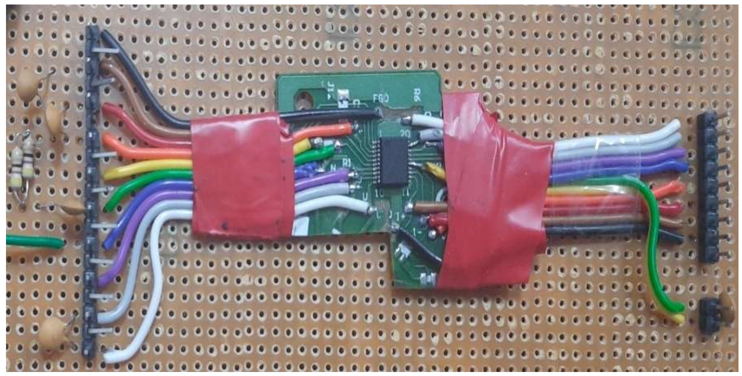

Fig. 3.10.1 Standalone ADC

Fig. 3.10.2 The degraded digital output performance of the ADC

The ADC is properly built on the KiCad tool along with supporting components to work at high frequencies in the second experiment, as shown in figure 3.7. Furthermore, steps have been taken to correct the defects in the previous circuit's design.

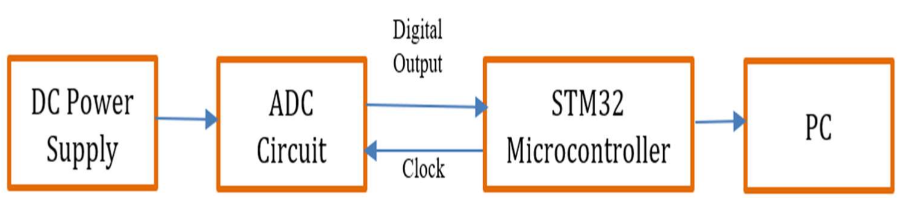

Fig. 3.11 Experimental setup for ADC Validation

The Block diagram of the experimental setup for ADC Validation is shown in figure 3.11. To validate the ADC circuit, a 130mV signal was applied as an input to it from the DC power supply. Binary word 193 is expected and the same is observed at the output of the buffer (74ACQ574). This data is acquired on the STM32 microcontroller and transferred to PC through UART. Using the same experimental setup by varying the input, the ADC's linearity curve is also plotted, as shown in Figure 3.12.1.

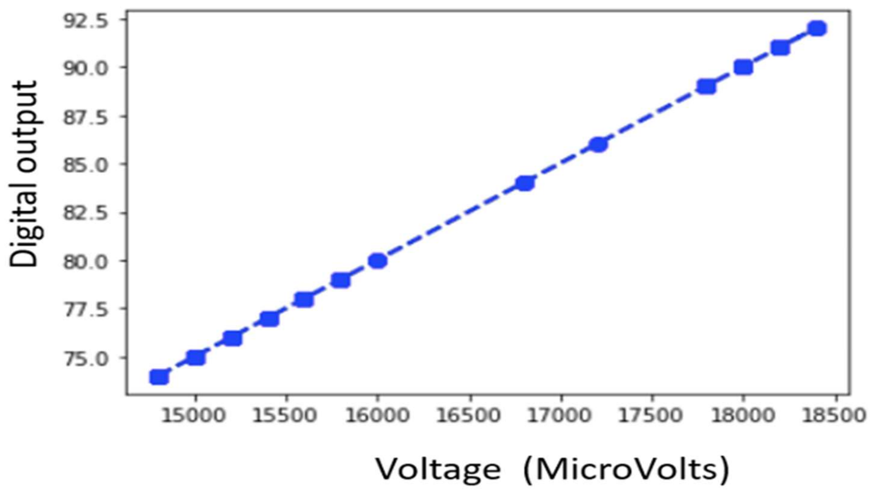

Fig. 3.12.1 The output response of the ADC w.r.t input

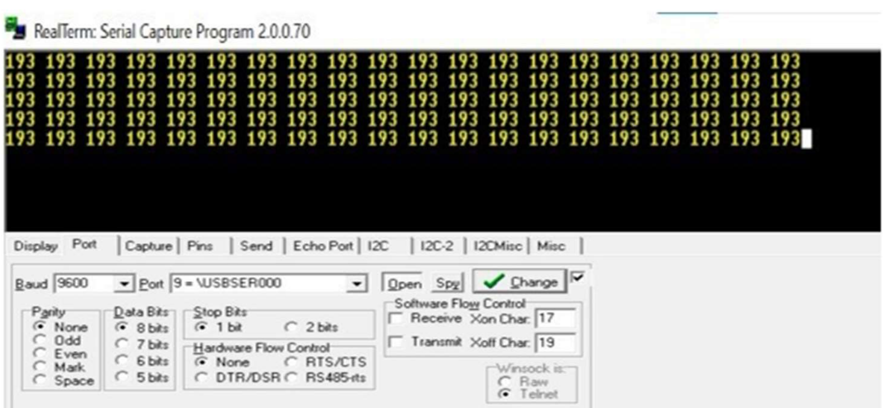

Fig. 3.12.2 The ADC output data on the real term terminal

The ADC's input range has been modified to further validate it by applying suitable DC at Vref pin. The microcontroller provided the clock to the ADC, which had a frequency of 5MHz and was used to digitise the input on every positive edge of the clock. On an oscilloscope, the digitised data of the ADC output for varied input was collected, and the waveforms may be seen in the following figures.

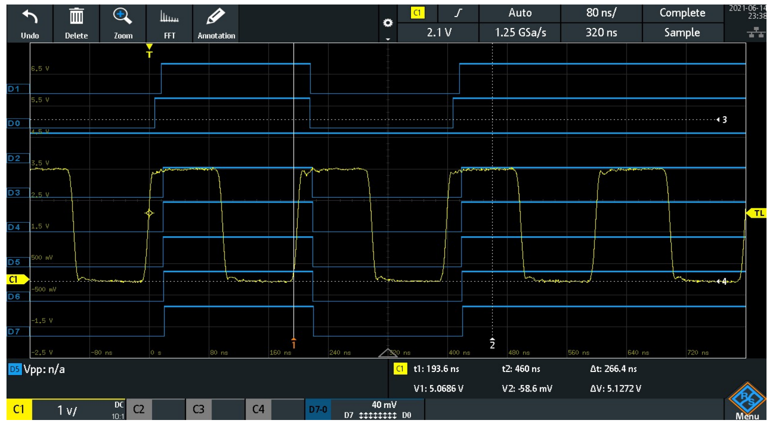

Fig. 3.13.1 The ADC output data on the oscilloscope for the input 1.6V

Fig. 3.13.2 The ADC output data on the oscilloscope for the input 2V

In figure 3.13 shows the input (yellow colored waveform) to the ADC and its output (blue colored waveform) is captured on the oscilloscope. From the above figures, it is clear that the output of ADC is clean and safe to use at high frequencies especially in photoacoustic applications.

3.7 Power Supply development

The compact and easily portable constant DC power supply is the primary requirement of the ADC circuit. The schematic diagram of ADC (Figure 3.7) clearly illustrates those two power supplies are needed for the ADC circuit. Also, the pre-amplifier needs two power supplies which are of low voltage and current ratings. Thus, a total of four power supplies was built in our laboratory and were used with PA experiments. Since the variation in power supply ratings can cause the change in gain of an amplifier or can produce the change in the operation of ADC thus, the developed power supplies must be highly stable. Although for the experiments, four different power supplies are designed, here in the thesis, the design of a basic regulated DC power supply is discussed.

In general, the AC voltage from the mains is step-downed by the transformer and is passed through the full-wave rectifier used with bridge configuration. Further, the ripples are minimized bypassing the voltage signal through the low pass filter. Subsequently, LM-317 a voltage regulator IC is used with the potentiometer to regulate the voltage to the desired value. To provide the stability, the voltage signal at the output of the voltage regulator is passed through the capacitive filter to nullify the ripples and provide a smooth DC voltage signal. Figure 3.10 shows the circuit diagram for a voltage regulator LM-317. In the circuit shown below, capacitors C1 and C2 are the ripple filters and the combination of potentiometer resistor R1 and a fixed resistor R2 is used to regulate the output DC voltage. The Arduino Nano microcontroller board is interfaced with the regulator IC and the voltage and current going into the load is displayed on the LCD. Also, the simulation results can be observed in the following figure 3.11.

This is the benefit of adjustable voltage regulators. It can be set to any voltage within the range supported by the voltage regulator.
The formula used in the voltage regulation of IC LM317 is given the following equation

$$V_{out} = 1.25 \times (1 + R1/240)$$

According to this formula, the greater the value of resistor R2, the greater the voltage output. The following are the values that will be used in the current setup to produce a stable 5V at the output. According to the formula above, the value of R2 must be 720 ohms for the LM317 to output 5 volts. In this case, one can bring up to 28 volts into the voltage regulator and regulate it down to 5 volts. Set up the above circuit and then use a multimeter to measure the output voltage by placing it across the C2 capacitor or the resistors; one will find it's very close to 5 volts.

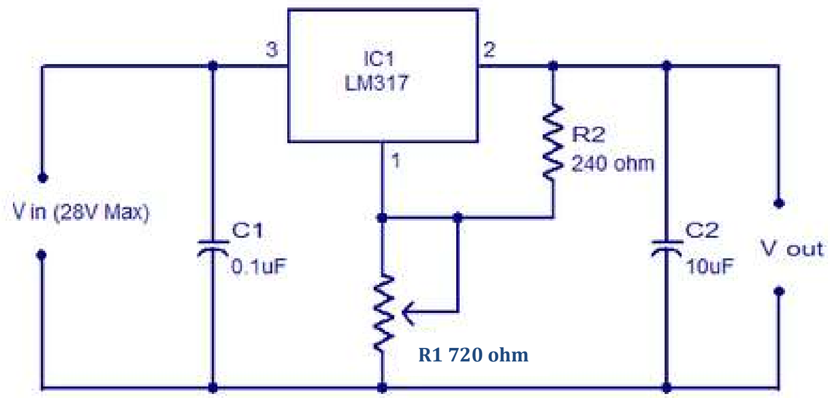

Fig. 3.14 Circuit diagram of a voltage regulator

The circuit design and simulation result of the voltage regulator can be seen in figures 3.13 and 3.14 respectively. In figure 3.14 shows the input (green colored waveform) to the voltage regulator is around 28V and its output (red-colored waveform) is constant 5V on proteus software.

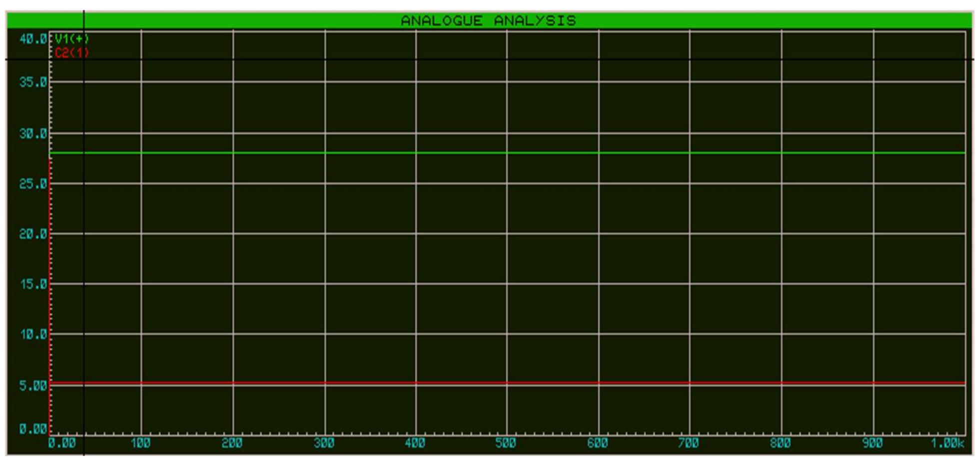

Fig. 3.15 simulation result for a voltage regulator

3.8 Summary

This chapter covers the design of high-frequency ADC, which is an essential part of the data acquisition system for photoacoustic applications. Several factors are considered when choosing an ADC, including the photodetector's bandwidth, input dynamic range, conversion rate, and so on. After choosing an ADC, the chapter aims to build a complete circuit for it. In particular, it focuses on developing a sharp transitioned high-frequency clock from the XOR gate and feeding it to the ADC. Once the ADC circuit design is complete, the PCB design is done using the KiCad software tool. The generated Gerber files from the PCB design are sent to fabrication, and thus the hardware for high-frequency ADC is realized. In addition, the ADC is validated by performing many experiments and plotting the linearity curve for it. Last but not least, the chapter also discusses the design and development of a reliable power supply for ADC is also designed and realized on hardware.

Chapter 4

Design & Development of Data Acquisition System: Acquisition using digital controller

Technology has enabled the use of microcontrollers and integrated circuits as required in the design of low-cost systems. In laboratories, a low-cost digital controller-based real-time data logging device can be used for measuring, tracking, and storing data for varying signals in the science and engineering streams. A common measurement application is data logging and recording. Data logging, in its most simple form, is the measurement and recording of physical or electrical parameters over time. Since oscilloscope can be used in the case of a digital controller, the usage of oscilloscope may not be so effective in all the applications. To generate tomographical images, it is necessary to use multiple sensors at different locations, particularly in imaging applications. The key concern is that we need multiple acquisition devices (e.g., oscilloscopes) for multiple sensors across the sample, which makes the device bulky and costly. Hence digital microcontrollers are preferred over oscilloscopes.

The design of an ADC circuit for digitizing a photoacoustic signal has been discussed in detail in Chapter 3. The conventional photoacoustic system encountered the same problem when capturing digitized photoacoustic signals from multiple sensors. The thesis describes the development of a low-cost DAQ using a microcontroller in order to overcome the mentioned challenges as well as to record the photoacoustic signal in order to provide offline signal processing and to replace oscilloscopes.

The following are the key challenges in the development of digital controller:

- The digital controller should be able to manage the ADC conversion and the acquisition rate of at least 40Mhz for the PA signal.
- To synchronize the ADC conversion rate with the GPIO sampling rate of the microcontroller. This is only possible if the digital controller is

capable of simultaneously acquiring data on the GPIO port and generating a clock for the ADC.

The following subsections cover the generation of a clock for the ADC and the acquisition of the digitized PA signal on the microcontroller.

4.1 Generation of Clock for ADC

4.1.1 Using FPGA

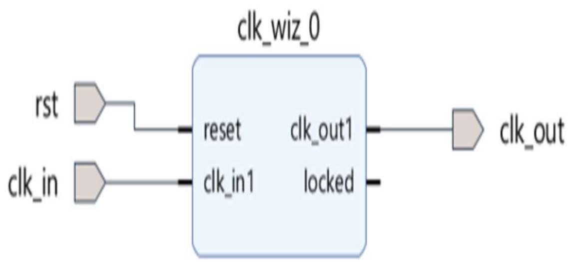

Fig. 4.1.1 Clocking wizard

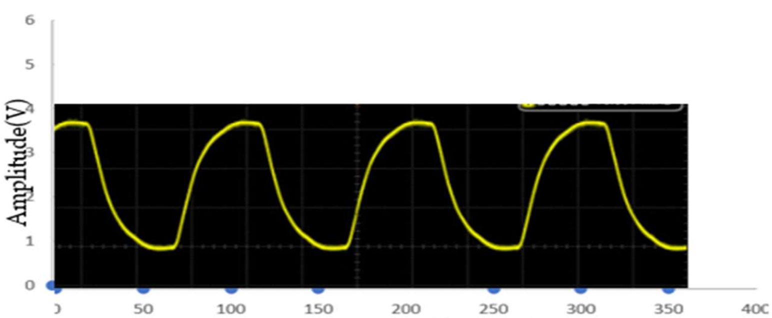

Fig. 4.1.2 *10 MHz Clock generation on FPGA GPIO pin*

Initially, the Basys 3 FPGA board is used to generate the clock for the ADC clock and to acquire the digitized PA signal. On one of the FPGA board's Port Pins, the clock is generated using the clocking wizard IP. The clocking wizard IP makes it easier to create HDL source code wrappers for clock circuits that are customized to our clocking needs. Figure 4.1.2 shows that at high frequencies, the clock produced on the port pin has a high slew rate, which can degrade the ADC's performance. The reason is that the FPGA's high-frequency GPIO pins have been allocated to on-chip devices rather than the Basys board's input/output ports [41]. Therefore, as an alternative solution, STM32 devices are explored for this application for creating a low-cost DAQ because they allow for high-speed communication through GPIO ports.

4.1.2 Using STM32 Microcontroller

The STM32F446RE microcontroller is used in this low-cost data acquisition method to collect data from an ADC that samples the amplified acoustic signal. The microcontroller is built around the high-performance Arm Cortex-M4 32-bit RISC core, and its on-chip bus can run up to 180 MHz [42], which is sufficient for acquiring the ADC output. Hence no signal loss is observed during the acquisition of high-frequency data output of ADC.

To validate whether the GPIO pins of the STM32F446RE microcontroller function for high frequency or not, a high-frequency clock for ADC is generated using the timer peripheral.

A timer (also known as a counter) is a piece of hardware used in many microcontrollers[42]. Their work is straightforward: they count up or down, depending on the configuration. One can apply a variety of settings to most timers to change the way they function. These settings are normally implemented in the microcontroller via other special function registers. Some of the usual hardware functions with timers are here:

- Output compare (OC): toggle a pin when a timer reaches a certain value
- Input capture (IC): calculate the number of counts of a timer between events on a pin
- Pulse width modulation (PWM): toggle a pin when a timer reaches a certain value and on rollover. By adjusting the on versus off time (duty cycle), one can effectively control the amount of electrical power going to another device.

These programmable timers have a time base unit that contains special function registers and they are Counter Register (TIMx_CNT), Prescaler Register

(TIMx_PSC), Auto-Reload Register (TIMx_ARR) [42]. The counter, the auto-reload register, and the Prescaler register can be written or read by software. The auto-reload register is preloaded. Writing to or reading from the auto-reload register accesses the preload register. The content of the preload register is transferred into the shadow register permanently or at each update event (UEV), depending on the auto-reload preload enable bit (ARPE) in the TIMx_CR1 register. The update event is sent when the counter reaches the overflow (or underflow when down counting) and if the UDIS bit equals 0 in the TIMx_CR1 register. It can also be generated by the software. That's how by using registers required clock frequency is generated on the GPIOs.

In this application, PWM mode is preferred over other modes to generate the clock for ADC since it supports generating high frequency with varying duty cycles.

Timer PWM mode

The timer is able to generate PWM in edge-aligned mode or center-aligned mode with a frequency determined by the value of the TIMx_ARR register, and a duty cycle determined by the value of the TIMx_CCRx register.

The following rules are followed in generating the GPIO pin that is connected to the timer peripheral.

• In up-counting, channelx is active as long as CNT< CCRx, otherwise it is inactive.

• In down-counting, channelx is inactive as long as CNT> CCRx, otherwise it is active.

To configure the timer in this mode:

1.Configure the output pin:

a) Select the output mode by writing CCS bits in the CCMRx register.

b) Select the polarity by writing the CCxP bit in the CCER register.

2. Select the PWM mode (PWM1 or PWM2) by writing OCxM bits in the CCMRx register.

3. Program the period and the duty cycle respectively in ARR and CCRx

registers.

4. Set the preload bit in the CCMRx register and the ARPE bit in the CR1 register.

5. Select the counting mode:

a) PWM edge-aligned mode: the counter must be configured up-counting or down counting.

b) PWM center-aligned mode: the counter mode must be center-aligned counting

mode (CMS bits different from '00').

6. Enable the capture compare.

7. Enable the counter.

Following the above rules, timer 2 is configured in PWM mode [42] and generated a high-frequency clock for the ADC, which is observed on the oscilloscope. The produced clock has a lower slew rate and is adequate for ADC conversion. Figure 4.2 shows the produced 30MHz on oscilloscope.

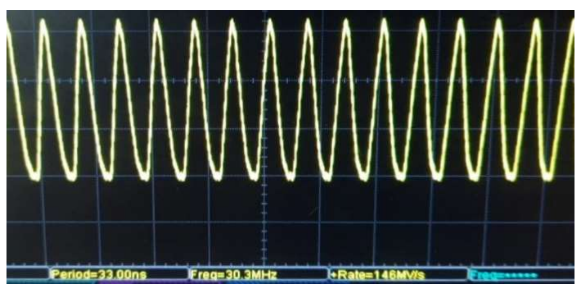

Fig. 4.2 Around 30MHz Clock generation for ADC on STM32 GPIO pin

4.2 Parallel synchronous transmission using GPIO and DMA

Using the embedded DMA IP, the STM32 MCUs can simulate parallel synchronous communication over the GPIO interface. In this data acquisition, a data clock is generated for DMA, and DMA samples the data present on GPIOs synchronously with the data clock. The transmitted frame contains up to 16 bits of data as well as a synchronous data clock. Timers are used to produce the data clock and monitor the transmission length (timeout, number of data packets sent).

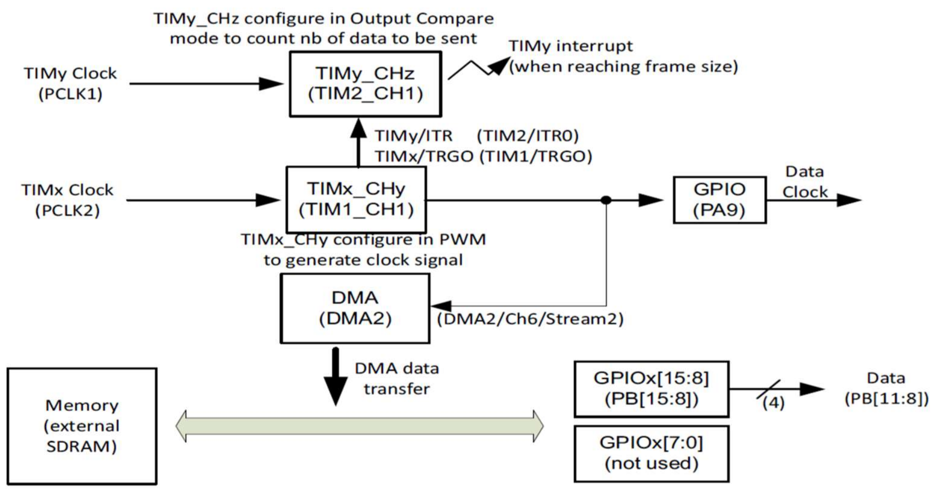

Fig. 4.3 STM32F446RE transmission architecture [42]

A timer (TIMx) configured in Pulse Width Modulation (PWM) Edge Aligned mode on one of its channels generates the data clock (CHy). So the TIMx_CHy output will toggle at a predefined frequency and duty cycle. The data clock frequency is computed from the TIMx Auto-reload register (TIMx_ARR) and timer frequency:

$$\mathrm{DataClockFreq} = (\mathrm{TIMxfreq}) / (\mathrm{TIMxARR} + 1)$$

The data clock duty cycle is a percentage computed from the TIMx capture/compare register (TIMx_CCRy):

$$\mathrm{DataClockDutycycle} = (\mathrm{TIMxCCRy}) / (\mathrm{TIMx1ARR} + 1) \times 100$$

The clock signal is output for TIMx_CHy and should be connected to an available GPIO. The same output is given as the ADC clock as well as the clock for DMA.

The TIMx CHy can generate DMA requests on each rising edge of the PWM data clock. As a DMA order, the TIMx OCyREF signal is used. In the DMA request table, the corresponding DMA request for the TIMx CHy channel should be open. To detect the end of transmission, a DMA counter is used. The frame size value is programmed into the DMA channel number of the data register (DMA CNDTR). When the DMA has finished sending the last data, a DMA Transfer Complete interrupt is created, and the TIMx data clock generator is shut down as soon as possible to prevent further clock toggling. The data present on the GPIOs must be transferred by DMA from the GPIOs to memory. That's how synchronization is achieved between DMA's GPIO sampling and ADC conversion.

4.3 Understanding STM32F446Rxx Bus Matrix

It is critical to understand the microcontroller's bus matrix when a specific application transfers data between two peripherals. In this application, the data sampled on the microcontroller's GPIO must be stored in memory. For this, understanding the microcontroller's is must.

The Bus Matrix connects master devices, known as initiators, to slave devices, known as targets. It decodes a broad range of addresses that correspond to a specific target. Depending on its functionality, the target (memory or peripherals) can have additional addresses. The main system is made up of a 32-bit multi-layer AHB bus matrix that can realize the interconnection depicted in figure 4.4. With the help of the bus matrix, the main bus to the controlled bus can be accessed, so that even during the simultaneous operation of multiple high-speed peripherals, the system can achieve concurrent access and efficient operation. It handles master-to-master control arbitration. A round-robin algorithm is used in the arbitration.

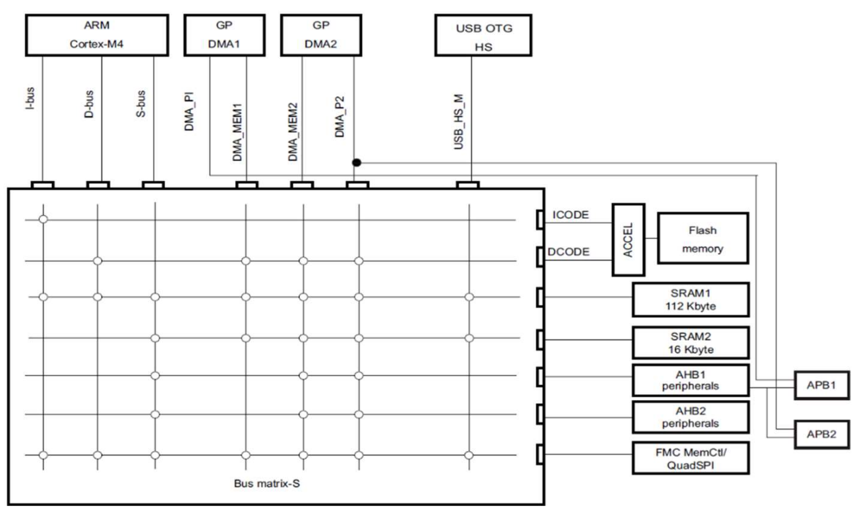

Fig. 4.4 Bus Matrix for STM32F44RXX Devices [42]

The DMA is used as the master in this application to collect the digitized PA data from the GPIO and store it in memory. The STM32F446RE microcontroller has multiple memories and DMAs. However, all of the DMAs in the STM32F446RE microcontroller doesn’t support data transfer from memories to AHB1 peripherals where GPIOs are connected via DMA. It is clear from the bus matrix that DMA1 does not accept data transfer because there is no path from AHB1 peripherals to memories. As a result, DMA2 is used to clear the path between AHB1pheriperals and memories.

4.4 Signal Acquisition on Microcontroller

The basic data flow scheme from ADC output to PC through the microcontroller is depicted in Figure 4.5.

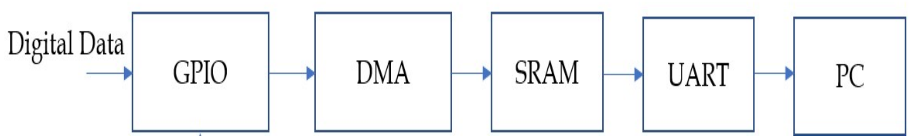

Fig. 4.5 Block diagram of dataflow on STM32F446RE

Figure 4.6 shows the configuration of the microcontroller's peripherals as well as the data flow from the sensor to the microcontroller's output. When the device is powered on, the peripherals of the microcontroller are configured and parameters are initialized. When the laser diode trigger, the microcontroller interprets it as an interrupt and produces the ENCODE instruction. This command is then sent to ADC, which converts an amplified PA signal to digital data. The digital data from the ADC is captured on the GPIO port and temporarily stored in SRAM1 via DMA 2. The microcontroller will average the stored data over time as well as keeps track of the cumulative number of acquisitions.

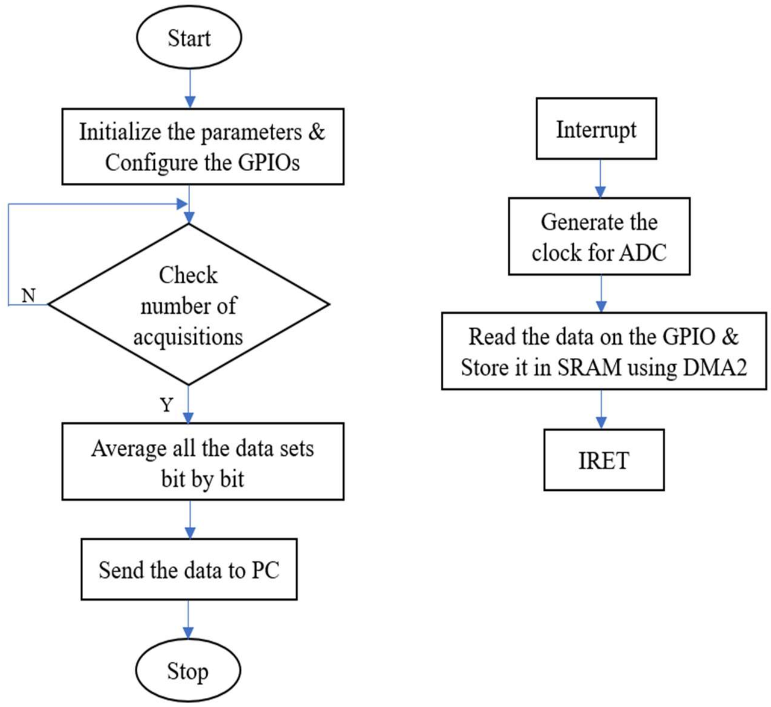

Fig. 4.6 Flow chart for the data movement in the DAQ

In this analysis, the time-averaging method is used to increase the signal-to-noise ratio (S/N ratio) of a signal by reducing the random noise associated with the PA signal. This method can be extended to any case where the signal stays constant over many measurement cycles. Here the PA signal is recorded several times and averaged in the microcontroller. Consequently, the noise will eventually cancel out because it contributes in a probabilistic fashion, while the net signal still contributes to a signal in the same direction. The time-averaged data is sent to the computer for reconstruction of the tomographic image.

The loop again starts upon checking the interrupt and the total number of acquisitions. If there is any reset on the microcontroller, it starts with the initial condition. The data flow closely observes the interrupt to acquire the data.

4.5 PCB design on KiCad

Figures 4.7 and 4.8 show the PCB design for the microcontroller done on the KiCad software tool. The same PCB design rules that have been addressed in Chapter 3 are followed in the design of this microcontroller.

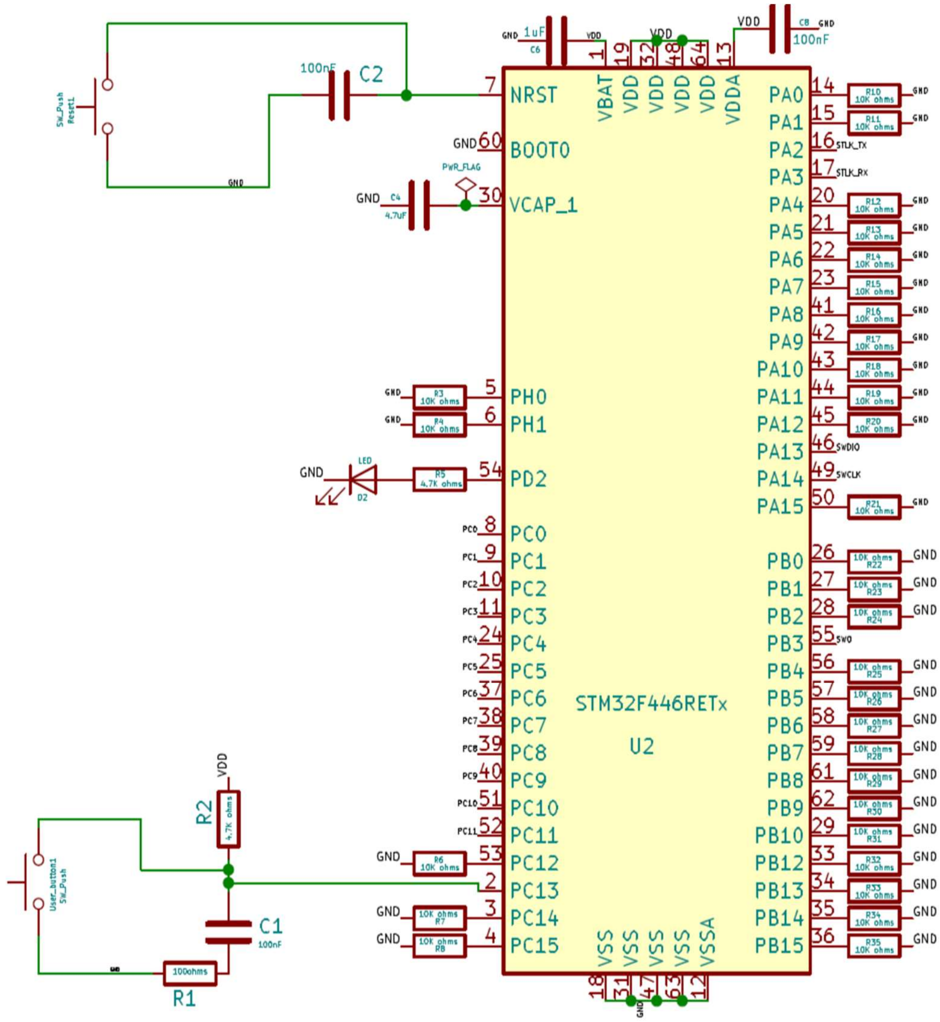

Fig. 4.7 schematic diagram for the STM32F446RE microcontroller circuit

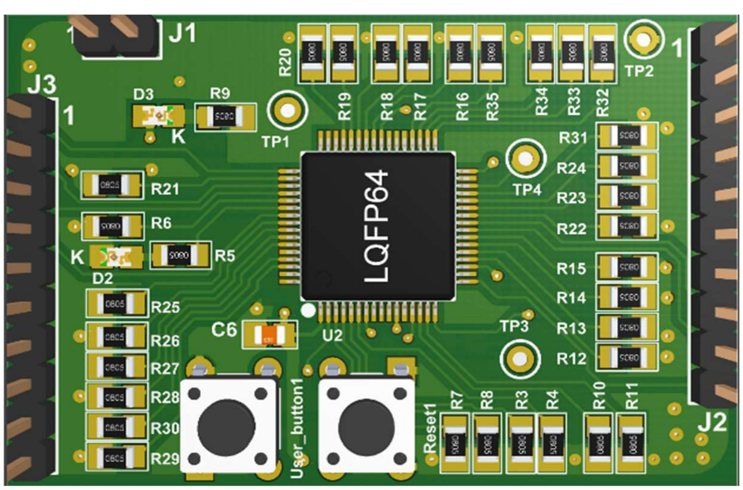

Fig. 4.8.1 Topper Copper Layer

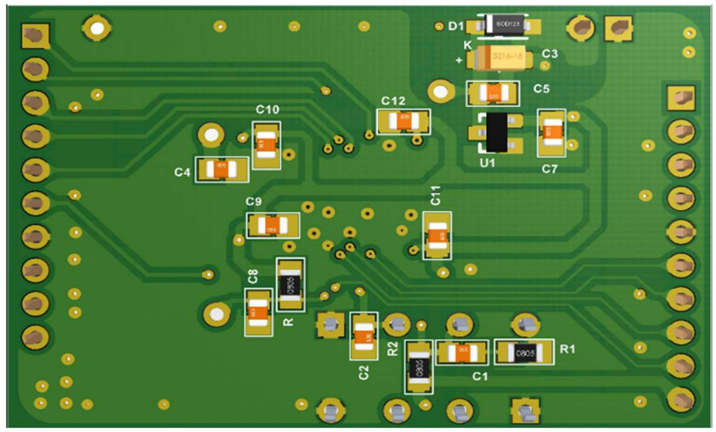

Fig. 4.8.2 Bottom Copper Layer

The in-house PCB design for the STM32 microcontroller has been developed. After the PCB is assembled, it is programmed in Keil software using Embedded C code.

4.6 Embedded C code for STM32 Microcontroller

The embedded C code for the data acquisition on the STM32F446RE microcontroller is given below.

```
#include "main.h"
#define OFFSET 0x800
#define DEST_ADDRESS (SRAM1_BASE + OFFSET)

TIM_HandleTypeDef htim2;
UART_HandleTypeDef huart2;
DMA_HandleTypeDef hdma_memtomem_dma2_stream0;

void SystemClock_Config(void);
static void MX_GPIO_Init(void);
static void MX_TIM2_Init(void);
static void MX_USART2_UART_Init(void);
static void MX_DMA_Init(void);
void my_Dma_Tc_cb(DMA_HandleTypeDef *pHandle);

int main(void)
{
  int i;
  uint8_t array[100];
  uint8_t* value = (uint8_t *)DEST_ADDRESS;

  HAL_Init();
  SystemClock_Config();
  MX_GPIO_Init();
  MX_TIM2_Init();
  MX_USART2_UART_Init();
  MX_DMA_Init();

  if(HAL_TIM_PWM_Start(&htim2, TIM_CHANNEL_1)!= HAL_OK)
```

```
            {
              Error_Handler();
            }
 while (1)
            {
            while(HAL_GPIO_ReadPin(GPIOC,GPIO_PIN_0)==GPIO_PIN_SET);
            HAL_DMA_Start(&hdma_memtomem_dma2_stream0,(uint32_t)&GPIOB-
>IDR,DEST_ADDRESS,100);

HAL_DMA_PollForTransfer(&hdma_memtomem_dma2_stream0,HAL_DMA_FULL_TRANSFER,
            HAL_MAX_DELAY);

            value = (uint8_t *)DEST_ADDRESS;
            for(i=0; i<100;i++)
                    {
                            array[i] = *value;
                            value = value+1;
                    }
            HAL_UART_Transmit(&huart2,array,(uint16_t)sizeof(array),HAL_MAX_DELAY);
            }

}

// @brief System Clock Configuration

void SystemClock_Config(void)
{
  RCC_OscInitTypeDef RCC_OscInitStruct = {0};
  RCC_ClkInitTypeDef RCC_ClkInitStruct = {0};

  __HAL_RCC_PWR_CLK_ENABLE();
  __HAL_PWR_VOLTAGESCALING_CONFIG(PWR_REGULATOR_VOLTAGE_SCALE1);
  /** Initializes the CPU, AHB and APB busses clocks
  */
  RCC_OscInitStruct.OscillatorType = RCC_OSCILLATORTYPE_HSI;
  RCC_OscInitStruct.HSIState = RCC_HSI_ON;
  RCC_OscInitStruct.HSICalibrationValue = RCC_HSICALIBRATION_DEFAULT;
  RCC_OscInitStruct.PLL.PLLState = RCC_PLL_ON;
  RCC_OscInitStruct.PLL.PLLSource = RCC_PLLSOURCE_HSI;
  RCC_OscInitStruct.PLL.PLLM = 8;
  RCC_OscInitStruct.PLL.PLLN = 180;
  RCC_OscInitStruct.PLL.PLLP = RCC_PLLP_DIV2;
  RCC_OscInitStruct.PLL.PLLQ = 2;
  RCC_OscInitStruct.PLL.PLLR = 2;
  if (HAL_RCC_OscConfig(&RCC_OscInitStruct) != HAL_OK)
  {
    Error_Handler();
  }

  if (HAL_PWREx_EnableOverDrive() != HAL_OK)
  {
    Error_Handler();
  }

  RCC_ClkInitStruct.ClockType = RCC_CLOCKTYPE_HCLK|RCC_CLOCKTYPE_SYSCLK
                              |RCC_CLOCKTYPE_PCLK1|RCC_CLOCKTYPE_PCLK2;
  RCC_ClkInitStruct.SYSCLKSource = RCC_SYSCLKSOURCE_PLLCLK;
  RCC_ClkInitStruct.AHBCLKDivider = RCC_SYSCLK_DIV1;
```

```
  RCC_ClkInitStruct.APB1CLKDivider = RCC_HCLK_DIV4;
  RCC_ClkInitStruct.APB2CLKDivider = RCC_HCLK_DIV2;

  if (HAL_RCC_ClockConfig(&RCC_ClkInitStruct, FLASH_LATENCY_5) != HAL_OK)
  {
    Error_Handler();
  }
}

// @brief TIM2 Initialization Function

static void MX_TIM2_Init(void)
{
        TIM_OC_InitTypeDef sConfigOC = {0};
        htim2.Instance = TIM2;
        htim2.Init.Prescaler = 2;
        htim2.Init.Period = 20;
        if (HAL_TIM_PWM_Init(&htim2) != HAL_OK)
        {
          Error_Handler();
        }
  sConfigOC.OCMode = TIM_OCMODE_PWM1;
  sConfigOC.Pulse = ( htim2.Init.Period * 60)/100;
  sConfigOC.OCPolarity = TIM_OCPOLARITY_HIGH;
  if (HAL_TIM_PWM_ConfigChannel(&htim2, &sConfigOC, TIM_CHANNEL_1) != HAL_OK)
  {
    Error_Handler();
  }
}

// @brief USART2 Initialization Function

static void MX_USART2_UART_Init(void)
{
  huart2.Instance = USART2;
  huart2.Init.BaudRate = 9600;
  huart2.Init.WordLength = UART_WORDLENGTH_8B;
  huart2.Init.StopBits = UART_STOPBITS_1;
  huart2.Init.Parity = UART_PARITY_NONE;
  huart2.Init.Mode = UART_MODE_TX_RX;
  huart2.Init.HwFlowCtl = UART_HWCONTROL_NONE;
  huart2.Init.OverSampling = UART_OVERSAMPLING_16;
  if (HAL_UART_Init(&huart2) != HAL_OK)
  {
    Error_Handler();
  }
}

// Configure DMA for memory to memory transfers

static void MX_DMA_Init(void)
{
  HAL_RCC_DMA2_CLK_ENABLE();
  hdma_memtomem_dma2_stream0.Instance = DMA2_Stream0;
  hdma_memtomem_dma2_stream0.Init.Channel = DMA_CHANNEL_0;
  hdma_memtomem_dma2_stream0.Init.Direction = DMA_MEMORY_TO_MEMORY;
  hdma_memtomem_dma2_stream0.Init.PeriphInc = DMA_PINC_DISABLE;
  hdma_memtomem_dma2_stream0.Init.MemInc = DMA_MINC_ENABLE;
```

```
  hdma_memtomem_dma2_stream0.Init.PeriphDataAlignment = DMA_PDATAALIGN_BYTE;
  hdma_memtomem_dma2_stream0.Init.MemDataAlignment = DMA_MDATAALIGN_BYTE;
  hdma_memtomem_dma2_stream0.Init.Mode = DMA_CIRCULAR;
  hdma_memtomem_dma2_stream0.Init.Priority = DMA_PRIORITY_HIGH;
  hdma_memtomem_dma2_stream0.Init.FIFOMode = DMA_FIFOMODE_ENABLE;
  hdma_memtomem_dma2_stream0.Init.FIFOThreshold = DMA_FIFO_THRESHOLD_FULL;
  hdma_memtomem_dma2_stream0.Init.MemBurst = DMA_MBURST_SINGLE;
  hdma_memtomem_dma2_stream0.Init.PeriphBurst = DMA_PBURST_SINGLE;
  if (HAL_DMA_Init(&hdma_memtomem_dma2_stream0) != HAL_OK)
  {
    Error_Handler( );
  }

  HAL_NVIC_SetPriority(DMA2_Stream0_IRQn, 0, 0);
  HAL_NVIC_EnableIRQ(DMA2_Stream0_IRQn);
}

void my_Dma_Tc_cb(DMA_HandleTypeDef *pHandle)
{

}

// @brief GPIO Initialization Function

static void MX_GPIO_Init(void)
{
  GPIO_InitTypeDef GPIO_InitStruct = {0};

  /* GPIO Ports Clock Enable */
  __HAL_RCC_GPIOC_CLK_ENABLE();
  __HAL_RCC_GPIOH_CLK_ENABLE();
  __HAL_RCC_GPIOA_CLK_ENABLE();
  __HAL_RCC_GPIOB_CLK_ENABLE();

  /*Configure GPIO pin Output Level */
  HAL_GPIO_WritePin(LD2_GPIO_Port, LD2_Pin, GPIO_PIN_RESET);
  GPIO_InitStruct.Pin = GPIO_PIN_0;
  GPIO_InitStruct.Mode = GPIO_MODE_INPUT;
  GPIO_InitStruct.Pull = GPIO_PULLUP;
  GPIO_InitStruct.Speed = GPIO_SPEED_FREQ_MEDIUM;
  HAL_GPIO_Init(GPIOC, &GPIO_InitStruct);
  GPIO_InitStruct.Pin = GPIO_PIN_0|GPIO_PIN_1|GPIO_PIN_2
                       |GPIO_PIN_3|GPIO_PIN_4|GPIO_PIN_5|GPIO_PIN_6
                       |GPIO_PIN_7;
  GPIO_InitStruct.Mode = GPIO_MODE_INPUT;
  GPIO_InitStruct.Pull = GPIO_PULLDOWN;
  GPIO_InitStruct.Speed =GPIO_SPEED_FREQ_MEDIUM;
  HAL_GPIO_Init(GPIOB, &GPIO_InitStruct);

  /*Configure GPIO pin : LD2_Pin */
  GPIO_InitStruct.Pin = LD2_Pin;
  GPIO_InitStruct.Mode = GPIO_MODE_OUTPUT_PP;
  GPIO_InitStruct.Pull = GPIO_NOPULL;
  GPIO_InitStruct.Speed = GPIO_SPEED_FREQ_MEDIUM;
  HAL_GPIO_Init(LD2_GPIO_Port, &GPIO_InitStruct);
}

// @brief TIM_PWM MSP Initialization
```

```
void HAL_TIM_PWM_MspInit(TIM_HandleTypeDef* htim_pwm)
{
 if(htim_pwm->Instance==TIM2)
 {
  GPIO_InitTypeDef GPIO_InitStruct = {0};
  __HAL_RCC_TIM2_CLK_ENABLE();
  __HAL_RCC_GPIOA_CLK_ENABLE();
  GPIO_InitStruct.Pin = GPIO_PIN_0;
  GPIO_InitStruct.Mode = GPIO_MODE_AF_PP;
  GPIO_InitStruct.Pull = GPIO_NOPULL;
  GPIO_InitStruct.Speed = GPIO_SPEED_FREQ_MEDIUM;
  GPIO_InitStruct.Alternate = GPIO_AF1_TIM2;
  HAL_GPIO_Init(GPIOA, &GPIO_InitStruct);
 }
}

// @brief UART MSP Initialization

void HAL_UART_MspInit(UART_HandleTypeDef* huart)
{
 GPIO_InitTypeDef GPIO_InitStruct = {0};
 if(huart->Instance==USART2)
 {
  __HAL_RCC_USART2_CLK_ENABLE();
  __HAL_RCC_GPIOA_CLK_ENABLE();
  GPIO_InitStruct.Pin = USART_TX_Pin|USART_RX_Pin;
  GPIO_InitStruct.Mode = GPIO_MODE_AF_PP;
  GPIO_InitStruct.Pull = GPIO_PULLUP;
  GPIO_InitStruct.Speed = GPIO_SPEED_FREQ_VERY_HIGH;
  GPIO_InitStruct.Alternate = GPIO_AF7_USART2;
  HAL_GPIO_Init(GPIOA, &GPIO_InitStruct);
 }
}
```

4.7 Summary

This chapter addresses the difficulties associated with interfacing a high-frequency ADC with a microcontroller. The challenges that have been addressed are the generation of a high-frequency clock and the synchronization of the DMA's GPIO sampling with the ADC conversion. The first challenge has been tried to be solved using Basys 3 FPGA but failed due to drawbacks present on the GPIOs. While holding low cost as the top priority, the STM32F446RE microcontroller has been chosen as a digital controller and addressed the above two stated challenges. Also, the in-house PCB design is done using the KiCad software tool. The generated Gerber files from PCB design are sent to fabrication and realized the hardware for digital controller for acquiring the photoacoustic signals.

Chapter 5

Design of a Prefilter

One of the thesis's goals, as discussed in Chapter 2, is to develop an analog front end (AFE) for photoacoustic signals. The AFE conditions the ultrasonic sensor's signal before interfacing with the analog-to-digital (A/D) converter. Due to the wide range of applications and their varying specifications, a general AFE architecture does not suit everything. An application-specific front-end for designs, on the other hand, is technically more superficial and less expensive. Similarly, indigenous AFE is designed for our application in the thesis. The main design elements of AFE are a Prefilter and an Amplifier. This chapter will go over the design of a Prefilter.

The following sections would cover an overview of an Analog front End and the design of a Prefilter.

5.1 Overview of Analog Front End

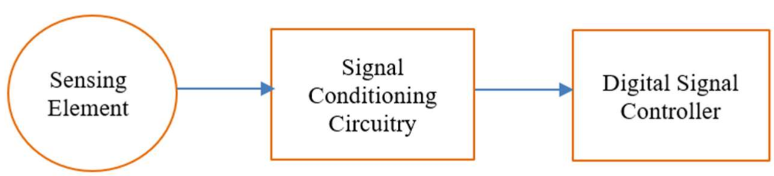

Fig. 5.1 Basic Sensor Signal Chain

An analog front-end (AFE) is a set of analog signal conditioning circuitry that uses sensitive analog amplifiers, often operational amplifiers, and prefilters to provide a configurable and flexible electronics functional block required to interface a variety of sensors to an antenna, analog-to-digital converter, or, in some cases, a microcontroller. The specific signal conditioning circuits required in a sensor application are determined by the type of sensor used. For example, A sensor that generates output voltages based on the magnitude of the physical parameter being measured would require different signal conditioning than a sensor that produces variable resistance. But, in general, certain signal conditioning requirements are common in sensor applications.

First, the sensor's output signals must be as noise-free as possible. Furthermore, the frequency content of the signal, or its bandwidth, must be limited to a certain range, based on some constraints that will be discussed shortly. This often necessitates the use of what is known as an Anti-Aliasing Filter.

Second, the sensors generate signals with low amplitudes, whether they are voltages, currents, or electric properties. The signal must be amplified in order to be processed accurately and to make the system more resistant to the effects of noise. In addition to being amplified, the signal may need to be translated to accommodate different ADC voltage references. Furthermore, many ADCs, particularly those contained within an MCU, only operate on unipolar inputs; that is, the input voltage cannot alternate between positive and negative levels with respect to Ground. In such cases, a Level Shifter is required.

As discussed in Chapter 3, the photoacoustic (PA) signals produced by the experiments have a very low amplitude of a few tens of microvolts due to the laser's low inherent power. It is also associated with noise. To match the input range of the ADC for digitizing the signal, a signal conditioning circuit that includes a prefilter and a highly sensitive and constant pre-amplifier gain of about 80 dB in the 1kHz-4MHz frequency range is required. Therefore, it is critical to building the AFE indigenously, which will meet the required specifications while also making the overall PA spectral response system very compact and cost-effective.

5.2 Design of Band-Pass filter

A filter is a device or technique which removes certain undesired components or features from a signal during signal processing. Filtering is a signal processing class, the defining property of the filters being that some portion of the signal has been completely or partially suppressed. For this application, a bandpass filter is proposed, since the photodetector center frequency is 3.5 MHz. The main feature of a bandpass filter is its capability to pass relatively unattenuated signals through a given range of frequencies known as the passband.

The active filters are well insulated and may provide high input impedance and low output impedance, independently of source and load impedances. When one wants to improve filter characteristics, multiple stages can be cascaded. Due to its high input impedance and its easily selectable gain, an operational amplifier in voltage-controlled voltage-source (VCVS) implementations are often used in active filter implementations. Here, one of the active filter designs based on VCVS is proposed in Sallen and Key topology. As such allows individual Sallen-key filter sections to be cascaded together to produce much higher order filters.

The main advantages of the Sallen-key filter design are [43]:

1. First and Second-order Filter Designs can be Easily Cascaded together
2. Low-pass and High-pass stages can be Cascaded Together
3. Each RC stage can have a different Voltage Gain
4. Replication of RC Components and Amplifiers
5. Second-order Sallen-Key Stages have Steep 40dB/decade roll-off than cascaded RC

However, there are some limitations to the basic Sallen-key filter design in that the voltage gain, A_V, and magnification factor, Q are closely related due to the use of an operational amplifier within the Sallen-key design.

The basic Sallen-key filter configuration can be used to implement different filter responses such as Butterworth, Chebyshev, or Bessel with the correct selection of RC filter network. It is also a 2^{nd}-order filter design that can be cascaded together with other RC stages to create higher-order filters. For instance, putting together a low-pass stage and a high-pass stage to create a Sallen and Key band-pass filter. The block of the bandpass filter can be seen in the below figure.

5.2.1 Design of Low-Pass filter

A Low-Pass filter is a filter that allows signals with frequencies lower than a specified cutoff frequency to pass while attenuating signals with frequencies higher than the cutoff frequency. The frequency response of the filter is determined by its design. A Sallen-Key Low-Pass circuit is shown in figure 5.2 below.

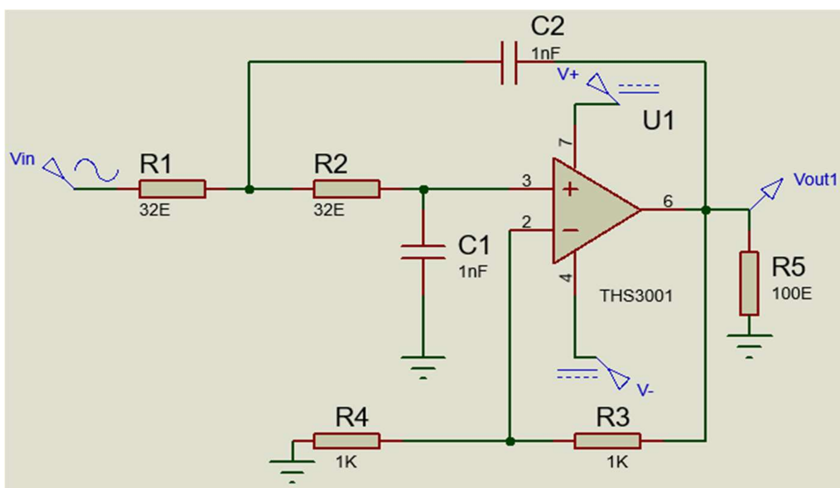

Fig. 5.2 Circuit design of Low-Pass Sallen-Key Filter

The standard frequency-domain equation for a second-order low-pass filter is represented by equation 5.2, where fc is the cutoff frequency (note that fc is the breakpoint between the passband and stopband, but is not always the –3 dB point) and Q is the quality factor. K, Q, and fc are calculated by comparing the Sallen-Key transfer function (equation 5.1) to the standard equation.

The ideal low-pass Sallen-Key transfer function is given below:

$$\frac{V_o}{V_i} = \frac{K}{s^2(R1R2C1C2)+s\big(R2C1+R1C2(1-K)\big)+1} \tag{5.1}$$

$$H_{LP} = \frac{K}{-(\frac{f}{fc})^2+\frac{jf}{Qfc}+1} \tag{5.2}$$

Where $K = 1 + \frac{R3}{R4}$, Cutoff frequency (f_c) = $\frac{1}{2\pi\sqrt{R1R2C1C2}}$

and Q = $\frac{\sqrt{R1R1C1C2}}{R1C1+R2C1+R1C2(1-K)}$

The circuit passes signals multiplied by a gain factor K when f<<fc and equation (5.2) reduce to K. Equation (5.2) reduces to –jKQ when f=fc, and signals are enhanced by the factor Q. When f>>fc, equation (5.2) reduces to $-K(\frac{f_c}{f})^2$, and signals are attenuated by the frequency ratio squared. The formula defines a second-order low-pass filter, with attenuation at higher frequencies increasing by a power of two. The design of a Low-Pass Sallen Key filter using the generally used simplification method of setting filter components as ratios is discussed below.

Letting R1=R2=R and, C1=C2=C results in:

$$f_c = \frac{1}{2\pi R} \qquad \text{and} \qquad Q = \frac{1}{3-K}$$

Now that fc and Q are independent of one another, the design is much simpler. Q is now determined by the circuit's gain. The choice of RC determines fc, and then the capacitor is chosen to calculate the resistor value. One minor disadvantage is that, because gain regulates Q in the circuit, additional gain or attenuation may be required to achieve the desired signal gain in the passband. K values close to 3 provide high Qs that are sensitive to variations in R3 and R4 values, resulting in Q=∞, and as values climb, Q becomes negative. Setting K=2 produces a Q of 1, and even in the worst-case condition with 1% resistors, the Q is 1.02.

Low Q values are required for the most commonly built filters, and this should rarely be a design concern.

For this application, the minimum upper cutoff frequency of the filter is chosen to be around 5MHZ. To achieve the required upper cutoff frequency, the following component values are used in the design of a low-pass Sallen-Key filter using THS3001 op-amp [44] show in figure 5.2.

Letting R3=R4=1kΩ results in:

$$K = 1 + \frac{R3}{R4} = 1 + \frac{1}{1} = 2$$

$$Q = \frac{1}{3 - K} = \frac{1}{3 - 2} = 1$$

$$f_c = \frac{1}{2\pi RC}$$

$$5\text{x}10^6 = \frac{1}{2\pi RC}$$

$$\text{RC} = 32\text{x}10^{-9}$$

If choosing C1=C2=1nf then R3=R4 will be 32Ω

By selecting the values of the above components, a Low-Pass Sallen Key filter circuit has been designed and the simulation results are shown in figure 5.3. The graph clearly shows that the filter's upper cutoff frequency is around 4.5MHz.

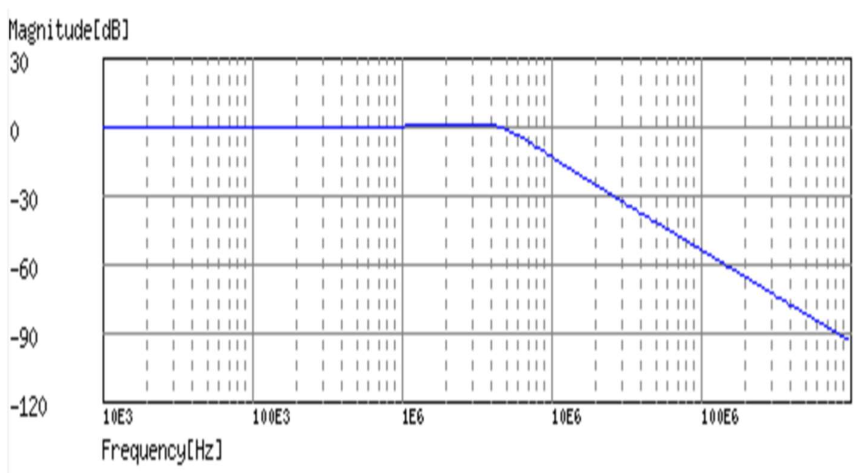

Fig. 5.3 Frequency Response of Low-Pass Sallen-Key Filter Using THS3001

5.2.2 Design of High-Pass filter

A High-Pass filter is a filter that allows signals with frequencies upper than a specified cutoff frequency to pass while attenuating signals with frequencies lower than the cutoff frequency. The frequency response of the filter is determined by its design. A Sallen-Key High-Pass circuit is represented in figure 5.4 below.

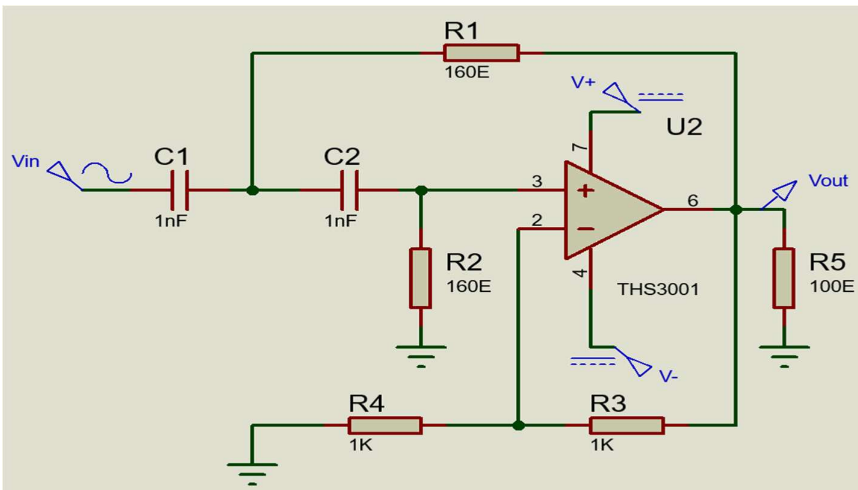

Fig. 5.4 Circuit design of High-Pass Sallen-Key Filter

The ideal high-pass Sallen-Key transfer function is given below:

$$\frac{V_o}{V_i} = \frac{K(s^2(R1R2C1C2))}{s^2(R1R2C1C2)+s\big(R2C1+R2C2+R1C2(1-K)\big)+1} \qquad (5.3)$$

$$H_{hp} = \frac{-K(\frac{f}{fc})^2}{-(\frac{f}{fc})^2+\frac{jf}{Qfc}+1} \qquad (5.4)$$

Where $K = 1+\frac{R3}{R4}$, Cutoff frequency $(f_c) = \frac{1}{2\pi\sqrt{R1R2C1C2}}$

and Q = $\frac{\sqrt{R1R1C1C2}}{R1C1+R2C1+R1C2(1-K)}$

The standard frequency-domain equation for a second-order high-pass filter is represented by Equation 5.4. K, Q, and fc are calculated by comparing the Sallen-Key transfer function to the standard equation.

The circuit passes signals multiplied by a gain factor K when f>>fc and equation (5.4) reduce to K. Equation (5.4) reduces to –jKQ when f=fc, and signals are enhanced by the factor Q. When f<<fc, equation (5.4) reduces to $-K(\frac{f_c}{f})^2$, and signals are attenuated by the frequency ratio squared. The formula defines a second-order high-pass filter, with attenuation at lower frequencies increasing by a power of two. The design of a High-Pass Sallen Key filter using the generally used simplification method of setting filter components as ratios is discussed below.

Letting R1=R2=R and, C1=C2=C results in:

$$f_c = \frac{1}{2\pi RC} \qquad \text{and} \quad Q = \frac{1}{3-K}$$

For this application, the maximum lower cutoff frequency of the filter is chosen to be around 1MHz. To achieve the required lower cutoff frequency, the following component values are used in the design of a high-pass Sallen-Key filter using THS3001 op-amp show in the figure 5.2.

Letting R3=R4=1kΩ results in:

$$K = 1 + \frac{R3}{R4} = 1 + \frac{1}{1} = 2$$

$$Q = \frac{1}{3-K} = \frac{1}{3-2} = 1$$

$$f_c = \frac{1}{2\pi RC}$$

$$1\text{x}10^6 = \frac{1}{2\pi RC}$$

$$\text{RC} = 160\text{x}10^{-6}$$

If choosing R3=R4=160Ω, C1=C2=1nF in the design.

By selecting the values of the above component, the filter circuit has been designed and the simulation results are shown in figure 5.5. The graph clearly shows that the filter's lower cutoff frequency is around 1MHz.

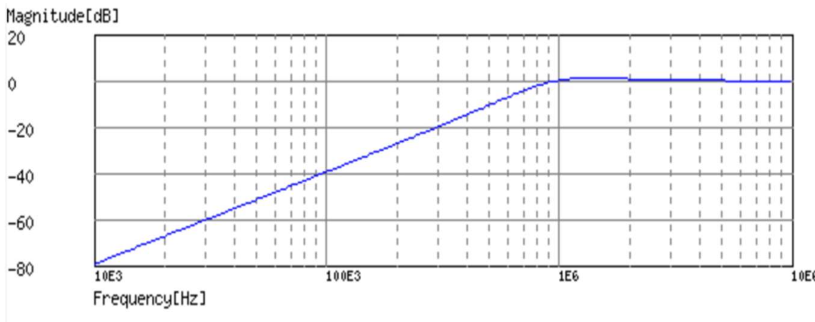

Fig. 5.5 Frequency Response of Band-Pass Sallen-Key Filter Using THS3001

5.2.3 Frequency response of the Band-Pass filter

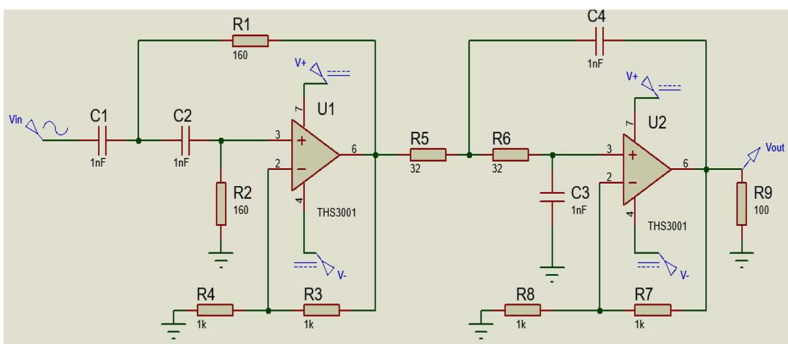

Fig. 5.6 Circuit design of Band-Pass Sallen-Key Filter

A Band-Pass filter is a filter that allows signals with a range of frequencies to pass through while attenuating signals at all other frequencies. Figure 5.6 depicts a simple active Band-Pass filter designed by cascading together a single Sallen-Key High-Pass Filter and a single Sallen-Key Low-Pass Filter for this application.

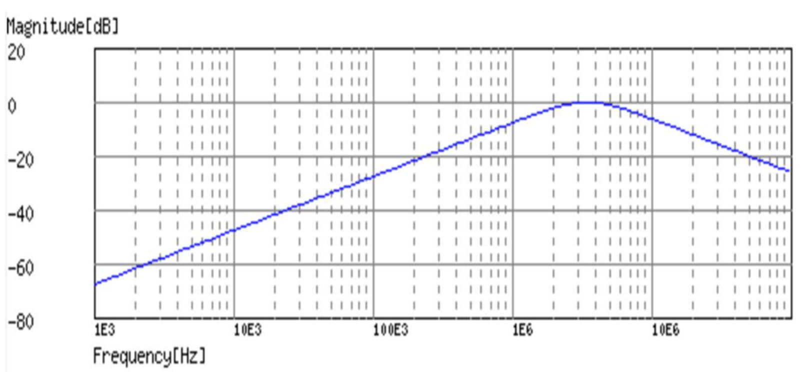

Fig. 5.7 Frequency Response of Band-Pass Sallen-Key Filter Using THS3001

Since the photodetector in this application has a center frequency of 3.5 MHz, a bandpass filter is proposed to pass relatively unattenuated signals in the frequency range of 1 MHz to 5 MHz while keeping the center frequency at 3.5 MHz. To obtain the given range, the lower and upper cutoff frequencies are calculated using the analysis done in the previous sections and observed the simulation result which is shown in figure 5.7. The graph clearly shows that the filter's center frequency is around 3.5 MHz. The filter's center frequency can also be adjusted for different applications by adjusting its passive component. This is how a simple band-pass filter for this application has been designed.

Chapter 6

Amplification of Ultrasonic Sound

The ultrasonic waves produced by the sample are detected by the ultrasonic detectors. As discussed in chapter 3, the amplitude of a typical blood sample's PA signal is 0.3 mV. This shows that the signal power required for acquisition is relatively low, and that great resolution is required to capture even minor changes. In addition, it also difficult to digitize the PA signal since most of the ADC's work in the range of millivolts to volts. Thus, to meet the input range of ADCs and to analyze the wave, the detected PA signal is needed to be amplified.

To convert a few tens of microvolts into a few volts of PA signal, amplification of at least 80 dB is required before being interfaced with an ADC. The following sections will go into the specifics of designing the amplifier to get the necessary gain.

6.1 Design of a Pre-amplifier circuit

As the SNR of the PA signal is very low, achieving high gain in the wide frequency range is very difficult using the single-stage amplifier due to the gain-bandwidth limitation and the amplifier's high noise level. Hence, in this study, a multi-stage amplifier is designed to attain an overall gain of 80dB. Also, for a low signal level at the input, the amplifier's high sensitivity would be the primary requirement.

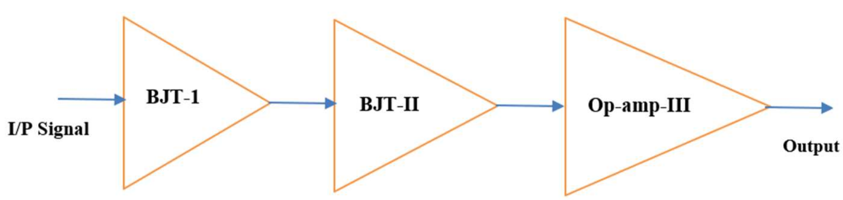

Fig. 6.1 Block diagram of 3 stage amplifier

A three-stage amplifier is designed in this amplifier configuration to achieve the desired gain over a large frequency range (1kHz - 4MHz) since the center frequency of the photodetector is 3.5 MHz in this application. Figure 6.1 shows the block diagram of the three-stage amplifier. Transistor technology is used to create signal amplification at all stages of the process. In the earlier stages, particularly in the high-frequency amplifier, these may be discrete devices. This arrangement also keeps costs down and increases the overall reliability of the system. Also, stage care must be taken when designing the multistage amplifier to avoid limiting the output. Otherwise, all input signals that exceed the limiting input produce the same level output, but the outputs are highly distorted. At this point, the amplifier is said to be saturated.

Here, the transistor (BJT) dependent amplifier stages are the first two stages, and the active (op-amp) phase is the third stage. Since a reliable voltage gain over a large frequency spectrum is the amplifier's primary requirement, a common emitter-based BJT amplifier with voltage divider bias is suggested. The final stage is the op-amp-based amplifier, which operates in inverting mode and delivers variable amplification with respect to the ADC input. The last stage is kept as an op-amp-based amplification stage because its output signal has to drive the AD9283 IC, which requires a low input impedance and a little high input current [38].

6.1.1 Single Stage BJT Amplifier

In its first stage of an amplifier, the BJT circuit is designed in common emitter mode to provide a high input impedance and a low output impedance. This configuration also provides a profoundly steady voltage gain.

The 2N2222 BJT is used in the first stage of the amplifier because it has a high-frequency response and requires low power to operate [45]. Figure 6.2 depicts the common emitter amplifier circuit of the BJT stage, which employs what is known as "Voltage divider Biasing." This type of biasing arrangement uses two resistors as a potential divider circuit. This method of biasing the transistor greatly reduces the effects of varying Beta by varying the base bias at a constant steady voltage level allowing for the best stability.

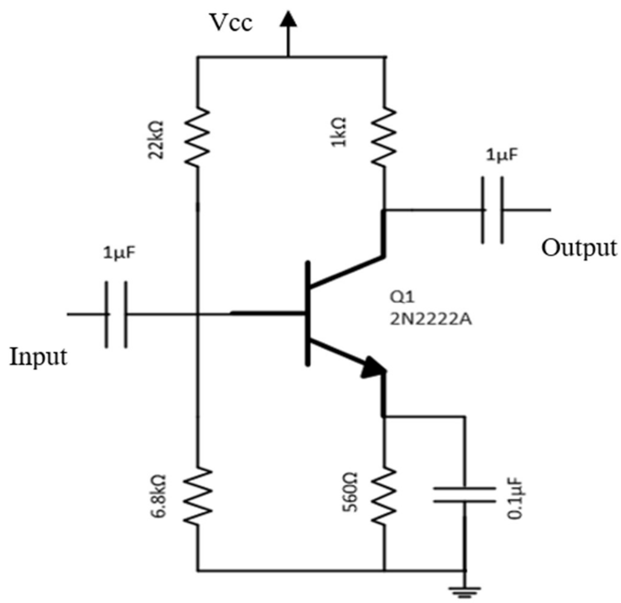

Fig. 6.2 Circuit diagram of Single Stage BJT Amplifier

To achieve the gain of at least 30dB each from each BJT stage the following value of components and supply voltage are used:
With R1 = 22kΩ, R2 = 6.8kΩ, Rc = 1kΩ, RE= 560Ω and Vcc = 6V,

VB can be given as-

VB = $(R2\ X\ \text{Vcc})\ /\ (R1+R2)$

VB = $(6.8\ X\ 6\ X\ 1000)\ /\ ((22+6.8)\ X\ 1000) \approx 1.41$ V

Since, VBE = 0.7V therefore,

VE= VB - VBE = 0.71V and IE = $VE\ /RE \approx 1.3$ mA.

re' = $VT\ /\ IE = 25mV\ /1.3mA \approx 21\Omega$

As the capacitor is connected across the emitter terminal thus the gain,
G1 = $RC\ /\ re' = 1000/21 = 48 \approx 33.5$dB

The first stage BJT gain was validated using Proteus software. In the simulation, a 50uV signal was applied as an input to the BJT and a 2.5mV amplified signal was observed at the output. Figure 6.3 depicts the simulation results of a first-stage BJT amplifier. It is important to note that the green and red waveforms in the figure represent the amplifier's input and output, respectively. The gain obtained is

$$\text{Gain} = \text{Vout} / \text{Vin} = 2.5\text{mV} / 50\text{uV}$$
$$\approx 33.98 \text{ dB}$$

The gain obtained in the simulation results is approximately equal to the theoretical one. The slight difference is due to parasitic capacitances at high frequencies. From the simulation results of single-stage BJT, it is evident that its output is insufficient to meet the ADC input.

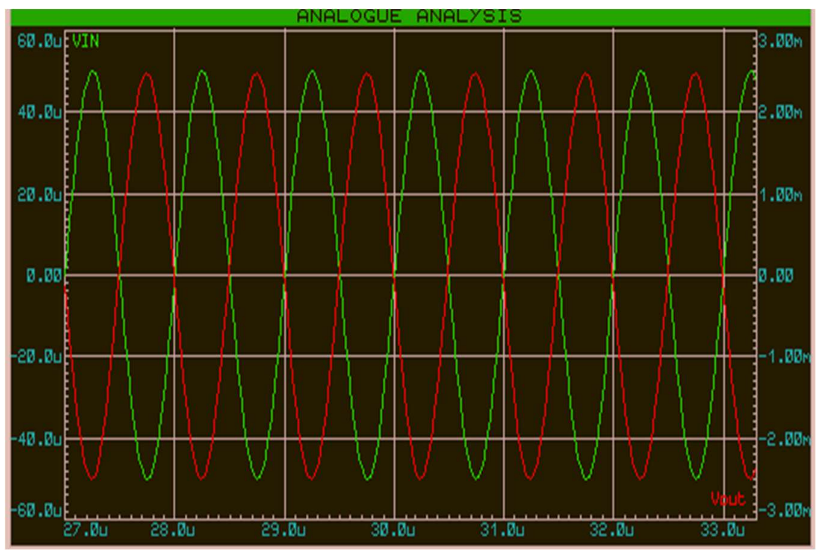

Fig. 6.9 Input and Output wave for a single stage BJT amplifier

6.1.2 Multistage Amplifier

As previously discussed in the chapter, the first two stages of the amplifier design are BJT, and both stages are identical to each other. The Proteus software was used to validate this two-stage BJT gain.

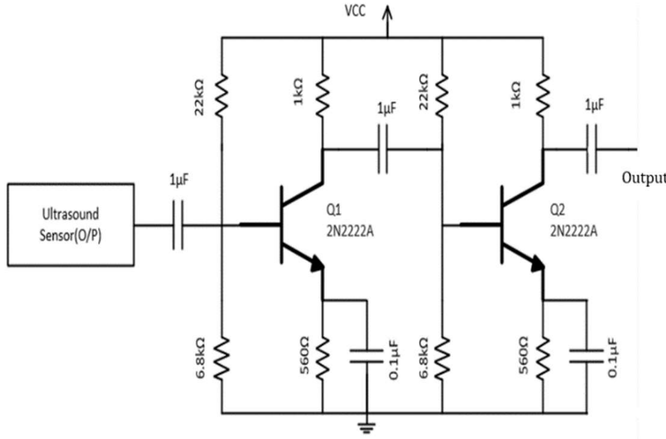

Fig. 6.4 Circuit diagram of two Stage BJT Amplifier

A 50uV signal was applied as an input to the two-stage BJT to simulate the circuit, and a 65mV amplified signal was observed at the output. It is important to note that the green and red waveforms in figure 6.5 represent the input and output of the amplifier, respectively. The gain obtained is

$$\text{Gain} = \text{Vout} / \text{Vin} = 65\text{mV} / 50\text{uV}$$
$$\approx 42.27 \text{ dB}$$

It is also worth noting that the first two stages are identical, but the overall gain is less than the sum of the individual gains of two BJT amplifiers. Because of the loading effect, this occurs in multistage amplifiers.

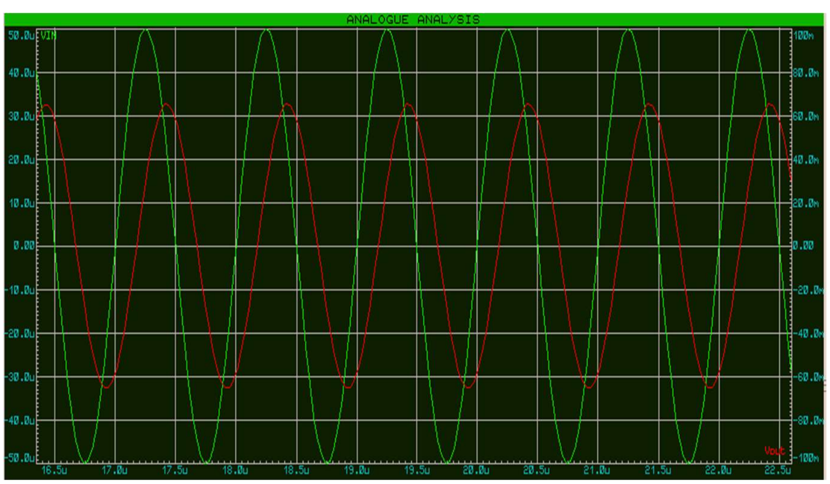

Fig. 6.5 Input and Output wave for a two-stage BJT amplifier

According to the simulation results of the two-stage BJT, its output is still insufficient to meet the ADC input. As a result, one more stage amplifier is recommended to meet the ADC input stage. As previously stated, the final stage is kept as an Op-amp to provide a low output impedance. The ultra-low noise, wideband op-amp (AD711) [45] is used in the final stage and can provide a good gain. It operates in inverting mode, with a variable feedback resistor and an input resistance of 200 ohms.

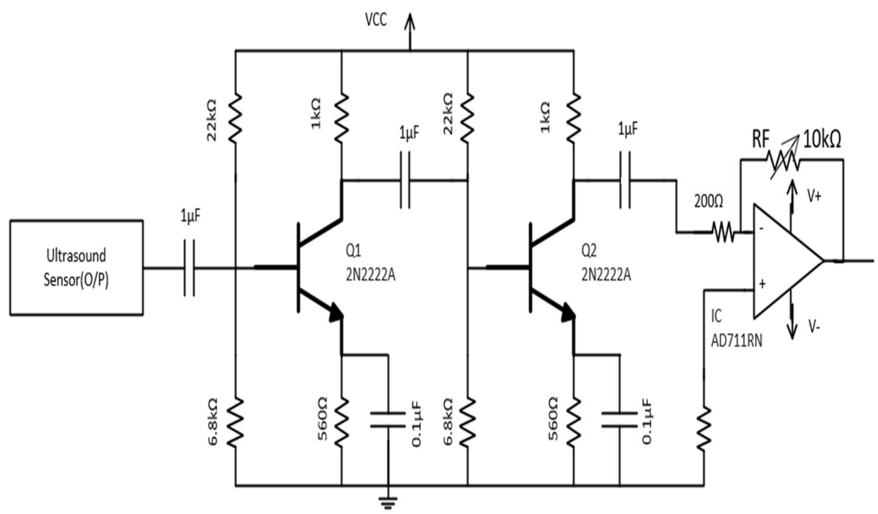

Fig. 6.6 Design of 3-Stage Amplifier

Figure 6.6 depicts the design of a three-stage amplifier. The coupling capacitors are used to cascade the three stages. These capacitors are used to isolate the AC signals from the DC bias voltage. This ensures that any additional amplifier stages do not affect the bias condition set up for the circuit to operate correctly, as the capacitors will only pass AC signals and block any DC component. The coupling capacitor values (C1, C2, and C3) have been chosen to be 1F. That is how the AC signal is superimposed on the biasing of the subsequent stages. Apart from coupling capacitors, bypass capacitors are also connected parallel with an emitter resistance to increase the voltage gain of the CE amplifier increases by eliminating extreme degeneration is developed in the amplifier circuit.

The aforementioned component values in the circuit diagram in figure 6.6 were used to provide a consistent gain of around 80dB across the entire frequency range of 1kHz - 4MHz. A variable feedback resistor (Rf) is also used in the amplifier's final stage to adjust the gain in reference to the ADC input.

A 50uV signal was applied as an input to the three-stage amplifier in the simulation, and a 460mV amplified signal was observed at the output. The simulation result of the amplifier is shown in Figure 6.7. It is important to note that the green and red waveforms in the figure represent the input and output of the amplifier, respectively. The gain obtained is

$$\text{Gain} = \text{Vout} / \text{Vin} = 460\text{mV} / 50\text{uV}$$
$$\approx 79.27 \text{ dB}$$

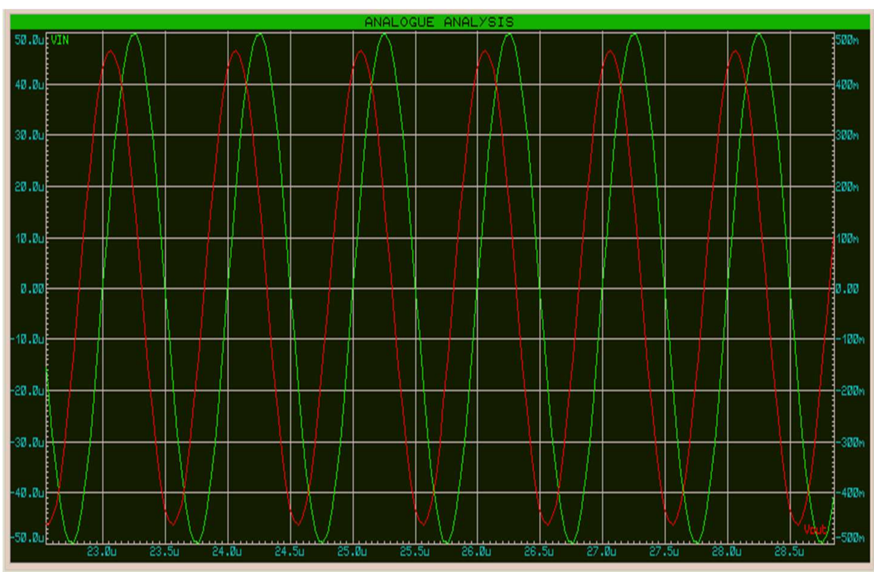

Fig. 6.7 Input and Output wave for a 3-stage amplifier

From the simulation result of the amplifier, it is clear that a 50uV signal is amplified to a 465mV signal. As discussed in chapter 3, the maximum amplitude of a typical blood sample's PA signal is 300uV. If the blood sample's PA signal is applied as input to the amplifier, the output would be 2.76V. Hence this voltage is sufficient to exploit the entire input range of an ADC.

Since the photodetector's center frequency is 3.5MHz in this application, the frequency response of the amplifier is observed on Proteus to validate whether it works for the PA experiments or not. Figure 6.8 shows the frequency response of the amplifier, which shows that the overall gain is constant and around 80dB in the frequency range of 1kHz-4MHz. After that, the gain gradually decreases, and at 5MHz, the overall gain decreases by approximately 18-20dB. The possible reason for the gain reduction could be the reduction in the capacitive reactance at higher frequencies. Besides, the parasitic capacitance at higher frequencies is significant, which can reduce the overall gain. Therefore, the developed pre-amplifier for the PA experiments is used to boost the PA signal amplitude before interfacing with an ADC.

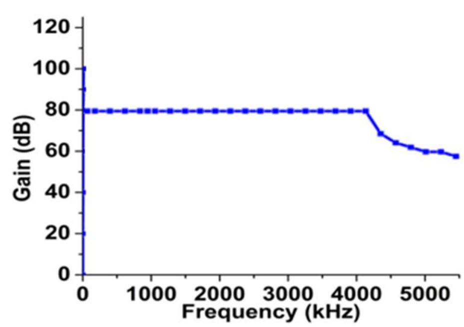

Fig. 6.8 Frequency response of the amplifier

6.2 Level Shifter and Buffer Amplifier

Since the amplified signal may include DC as a result of capacitances at different amplification stages, the signal may also need to be adjusted to suit different ADC voltage references. Also, few ADCs only operate on unipolar inputs; that is, the input voltage cannot alternate between positive and negative levels with respect to the Ground. In such cases, a Level Shifter, a form of inverting op-amp circuit, is needed for the amplifier's output before interfacing with an ADC. Another special signal conditioning circuit that may be required is a Buffer Amplifier, which is an op-amp circuit that is used to transfer a voltage from a circuit with high output impedance to a circuit with low input impedance. Circuit diagrams for the buffer and level shifter can be observed in figure 6.9.

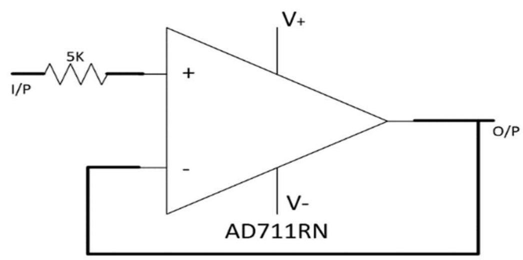

Fig. 6.9.1 Buffer

The formula used in the calculation of the Buffer's output is given the following equation

$$Vout=Vin$$

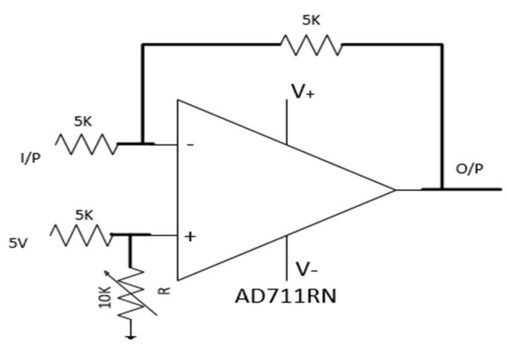

Fig. 6.9.2 level Shifter

The formula used in the calculation of the Level shifter's output is given the following equation

$$Vout = (10*R / (R+5)) - Vin$$

6.3 Summary

This chapter discussed the problems in ADC interfacing with the input PA signal, as well as the requirement to amplify the detected PA signal. In this application, the PA signal must be amplified by at least 80 decibels before being interfaced with an ADC. The three-stage amplifier was used to produce the desired gain. The limitations of utilizing a single-stage amplifier, as well as the justifications for employing a multistage amplifier, have also been discussed. Besides, each stage's circuit analysis and simulation results have been validated. It was proven by the frequency response of the amplifier that it was safer to use with the photodetector present in this application. Last but not least the design of the level shifter and the buffer, has also been discussed.

Chapter 7

Conclusion and future work

7.1 Conclusion

In the thesis, the photoacoustic imaging technique and its associated instrumentation have been studied in detail. It also discusses the limitations of conventional photoacoustic instrumentation. To overcome those limitations, a low-cost and portable photoacoustic instrumentation has been proposed.

The key motivation behind the proposed system is the need for a fast and reliable analog front-end design (AFE) to amplify the photoacoustic signal whose amplitude is in few microvolts as well as to replace oscilloscopes present in conventional photoacoustic instrumentation with compact DAQ to acquire the photoacoustic signal for further processing. This system includes two key designs, which are as follows:

- Design of Analog front-end (AFE)
- Acquisition of Photoacoustic Signal on the digital controller

In AFE design, the limitations of a general AFE architecture and the need for an application-specific front-end for designs are discussed. It also addressed the issues with ADC interfacing with the input PA signal, as well as the need to amplify the detected PA signal. On that note, an indigenous AFE has been designed in the project to signal condition the photodetector's output. AFE's design includes a prefilter as well as a highly sensitive and constant pre-amplifier gain of approximately 80 dB. Especially in the design of the amplifier, the three-stage amplifier was utilized to achieve the desired gain. The limitations of utilizing a single-stage amplifier, as well as the justifications for employing a multistage amplifier, have also been discussed. The frequency response of this multistage amplifier also showed that it was safer to use with the photodetector in this application.

After signal conditioning the photoacoustic signal, it has been digitized using high-frequency AD9283 ADC, which is an important component of the data acquisition system for photoacoustic applications. In addition, hardware for ADC is realized is validated by performing many experiments and plotting the linearity curve for it.

To execute offline signal processing, the digitised data is stored in digital controllers, which have replaced multiple oscilloscopes in the case of multiple sensors. Digital controllers were used to make the device more compact and portable. In this application, the STM32F446RE microcontroller is utilized as a digital controller to obtain high-speed and accurate digitized data. The thesis also addresses the difficulties associated with interfacing a high-frequency ADC with a microcontroller. The challenges that have been addressed are the generation of a high-frequency clock and the synchronization of the DMA's GPIO sampling with the ADC conversion.

The data saved in the STM32F446RE microcontroller is time-averaged over desired frames to reduce random noise in the signal before being sent to a computer for reconstruction of a tomographic image of biological tissue for diagnostic purposes.

In summary, all the designs have been extensively explored and realized the hardware for the proposed data acquisition system for photoacoutic applications. Also, the detailed description of those designs along with their input/output waveforms diagrams have been articulated in the thesis.

7.2 Prospects

The future work in this DAQ can be analyzing the ultrasonic waves detected by the detector. These waves can be analyzed to produce images of the biological sample. Different biological samples can be analyzed using different voltage functions for laser excitation. This type of Photoacoustics Imaging has various applications in the industry today. Some of the biomedical applications include:

Brain lesion detection

Photoacoustics Tomography, or PAT, can detect soft tissues in the brain with varying optical absorption qualities.

Hemodynamics monitoring

Since Hbo2 and Hb are the dominant absorbing compounds in biological tissues in the visible spectral range, multiple wavelength photoacoustic measurements can be used to reveal the relative concentration of these two chromophores. Thus, the relative total concentration of hemoglobin (Hbt) and the hemoglobin oxygen saturation (so2) can be derived. Therefore, cerebral dynamic changes associated with brain function can be successfully detected with PAT.

Other Applications

Photoacoustic imaging was introduced recently in the context of artwork diagnostics with an emphasis on the uncovering of hidden features such as underdrawings or original sketch lines in paintings. Photoacoustic images, collected from miniature oil paintings on canvas, illuminated with a pulsed laser on their reverse side, revealed the presence of pencil sketch lines coated over by several paint layers.

Potential applications also include the clinical assessment of vascular disease and skin abnormalities. The technique also has important applications as a research tool in the basic life sciences for undertaking molecular and genomic imaging studies, for example studying tumour physiology.

In addition to biomedical photoacoustic imaging, a range of ultrasound field measurement and imaging tools based upon the use of Fabry Petrol polymer film sensing interferometers is being developed. These include a miniature wideband fiber optic hydrophone for characterizing medical and industrial ultrasound fields and high-speed 2D arrays for field visualization and imaging applications in medicine and industrial NDT.

These types of low-cost and compact DAQs also play a vital role in portable devices. The portable medical device use is rapidly expanding as advancements in wireless technologies have increased patient's mobility at a hospital or home.

References

[1] Jiang, Daohuai, Yifei Xu, Yongjian Zhao, Hengrong Lan, and Fei Gao. "Low-Cost Photoacoustic Tomography System Based on Water-Made Acoustic Delay-Line." In 2019 IEEE International Ultrasonics Symposium (IUS), pp. 2369-2372. IEEE, 2019.

[2] Mahzan, N. N., et al. "Design and development of an arduino based data logger for photovoltaic monitoring system." Int. J. Simul. Syst. Sci. Technol 17.41 (2017): 15-1.

[3] González, Alejandro, José Luis Olazagoitia, and Jordi Vinolas. "A low-cost data acquisition system for automobile dynamics applications." Sensors 18.2 (2018): 366.

[4] Salgado, Débora Pereira, et al. "A QoE assessment method based on EDA, heart rate and EEG of a virtual reality assistive technology system." Proceedings of the 9th ACM Multimedia Systems Conference. 2018.

[5] Valluru, Keerthi S., Bhargava K. Chinni, Navalgund A. Rao, Shweta Bhatt, and Vikram S. Dogra. "Basics and clinical applications of photoacoustic imaging." Ultrasound Clinics 4, no. 3 (2009): 403-429.

[6] Manohar, Srirang, and Daniel Razansky. "Photoacoustics: a historical review." Advances in optics and photonics 8, no. 4 (2016): 586-617.

[7] Beard, Paul. "Biomedical photoacoustic imaging." Interface Focus 1, no. 4 (2011): 602-631.

[8] Wang, Lihong V., and Hsin-I. Wu. Biomedical optics: principles and imaging. John Wiley & Sons, 2012.

[9] C. Zhang and Y. Wang, “Comparison of Various Imaging Modes for Photoacoustic Tomography”, in 13th International Conference on Biomedical Engineering, Springer, Berlin, Heidelberg, 2009, pp. 121–124.

[10] De Montigny, Etienne. "Photoacoustic Tomography: Principles and applications." Department of Physics Engineering, polytechnic school Montreal (2011).

[11] A. G. Bell, “On the production and reproduction of sound by light,”

Am. J. Sci., vol. Series 3 Vol. 20, no. 118, pp. 305–324, Oct. 1880.
[12] Harren, Frans JM, Julien Mandon, and Simona M. Cristescu. "Photoacoustic spectroscopy in trace gas monitoring." Encyclopedia of Analytical Chemistry: Applications, Theory, and Instrumentation (2006).
[13] McClelland, John F., and Richard N. Kniseley. "Photoacoustic spectroscopy with condensed samples." Applied optics 15, no. 11 (1976): 2658-2663.
[14] Oralkan, Omer, A. Sanli Ergun, Jeremy A. Johnson, Mustafa Karaman, UtkanDemirci, KambizKaviani, Thomas H. Lee, and Butrus T. Khuri-Yakub. "Capacitive micromachined ultrasonic transducers: Next-generation arrays for acoustic imaging." IEEE transactions on ultrasonics, ferroelectrics, and frequency control 49, no. 11 (2002): 1596-1610.
[15] Maslov, Konstantin, Hao F. Zhang, Song Hu, and Lihong V. Wang. "Optical-resolution photoacoustic microscop1y for in vivo imaging of single capillaries." Optics Letters 33, no. 9 (2008): 929-931.
[16] Wang, Lihong V. "Tutorial on photoacoustic microscopy and computed tomography." IEEE Journal of Selected Topics in Quantum Electronics 14, no. 1 (2008): 171-179.
[17] A. A. Vives, Piezoelectric Transducers and Applications. Springer Science & Business Media, 2013.
[18] J. Tichý, J. Erhart, E. Kittinger, and J. Prívratská, Fundamentals of Piezoelectric Sensorics: Mechanical, Dielectric, and Thermodynamical Properties of Piezoelectric Materials. Springer
[19] C. G. A. Hoelen and F. F. M. De Mul, “A new theoretical approach to photoacoustic signal generation,” J. Acoust. Soc. Am., vol. 106, no. 2, pp. 695–706, 1999.
[20] B. E. Treeby and B. T. Cox, “k-Wave: MATLAB toolbox for the simulation and reconstruction of photoacoustic wave fields,” J. Biomed. Opt., vol. 15, no. 2, pp. 21314-21314–12, 2010.
[21] C. Li and L. V. Wang, “Photoacoustic tomography and sensing in biomedicine,” Phys. Med. Biol., vol. 54, no. 19, p. R59, 2009.
[22] S. H. Holan and J. A. Viator, “Automated wavelet denoising of

photoacoustic signals for circulating melanoma cell detection and burn image reconstruction,” Phys. Med. Biol., vol. 53, no. 12, p. N227, 2008.
[23] Z. Ren, G. Liu, and Z. Xiong, “Photoacoustic signals denosing of the glucose aqueous solutions using an improved wavelet threshold method,” 2016, vol. 10153, p. 101530A–101530A–9.
[24] G. T. Herman, Fundamentals of Computerized Tomography: Image Reconstruction from Projections. Springer Science & Business Media, 2009.
[25] J. D. Bronzino, Biomedical Engineering Handbook. CRC Press, 1999.
[26] B. E. Treeby, E. Z. Zhang, and B. T. Cox, “Photoacoustic tomography in absorbing acoustic media using time reversal,” Inverse Probl., vol. 26, no. 11, p. 115003, 2010.
[27] Y. Hristova, P. Kuchment, and L. Nguyen, “Reconstruction and time reversal in thermoacoustic tomography in acoustically homogeneous and inhomogeneous media,” Inverse Probl., vol. 24, no. 5, p. 55006, 2008.
[28] K. Firouzi, B. T. Cox, B. E. Treeby, and N. Saffari, “A firstorder k-space model for elastic wave propagation in heterogeneous media,” J. Acoust. Soc. Am., vol. 132, no. 3, pp. 1271–1283, 2012.
[29] Y. Jing, T. Wang, and G. T. Clement, “A k-space method for moderately nonlinear wave propagation,” IEEE Trans. Ultrason. Ferroelectr. Freq. Control, vol. 59, no. 8, pp. 1664–1673, 2012.
[30] J. Gamelin et al., “Curved array photoacoustic tomographic system for small animal imaging,” J. Biomed. Opt., vol. 13, no. 2, p. 24007, 2008.
[31] C. G. A. Hoelen and F. F. M. De Mul, “A new theoretical approach to photoacoustic signal generation,” J. Acoust. Soc. Am., vol. 106, no. 2, pp. 695–706, 1999.
[32] Gorey, Abhijeet, Deblina Biswas, AnshuKumari, Sharad Gupta, Norman Sharma, George CK Chen, and Srivathsan Vasudevan. "Application of continuous-wave photoacoustic sensing to red blood cell morphology." Lasers in medical science (2018): 1-8.
[33] C. Hoelen, F. De Mul, R. Pongers, and A. Dekker, “Three-

dimensional photoacoustic imaging of blood vessels in tissue," Opt.Lett., vol. 23, no. 8, pp. 648–650, 1998.

[34] M. Heijblom, W. Steenbergen, and S. Manohar, "Clinical photoacoustic breast imaging: the Twente experience," IEEE Pulse, vol. 6, no. 3, pp. 42–46, 2015.

[35] Biswas, Deblina, Abhijeet Gorey, Goerge CK Chen, Norman Sharma, and SrivathsanVasudevan."Investigation of diseases through red blood cells' shape using photoacoustic response technique." In Dynamics and Fluctuations in Biomedical Photonics XII, vol. 9322, p. 93220K.International Society for Optics and Photonics, 2015.

[36] Zou C, Wu B, Dong Y, Song Z, Zhao Y, Ni X, Yang Y, Liu Z. Biomedical photoacoustics: fundamentals, instrumentation and perspectives on nanomedicine. International journal of nanomedicine. 2017; 12:179.

[37] Digi-Key (2018), www.digikey.in/en/articles/iot-microcontrollers-have-adcs-know-when-apply-an-external-adc/

[38] AD9283 datasheet

[39] SN74LVC datasheet

[40] KiCad (1992), www.kicad.org/

[41] Basys 3 board datasheet

[42] STM32F446RE datasheet

[43] Saraga, W. "Sensitivity of 2nd-order Sallen-key-type active RC filters." Electronics letters 3.10 (1967): 442-444.

[44] THS3001 Op-amp datasheet

[45] AD711 Op-amp datasheet